Numerical simulations of radar echoes rule out basal CO_2 ice deposits at Ultimi Scopuli, Mars.

Roberto Orosei[1], Graziella Caprarelli[2]*, Sebastian Lauro[3], Elena Pettinelli[3], Marco Cartacci[4], Andrea Cicchetti[4], Barbara Cosciotti[3], Alessandro De Lorenzis[5], Giorgio De Nunzio[6,7], Elisabetta Mattei[3], Carlo Nenna[8], R. Noschese[4], Francesco Soldovieri[9].

[1]. Istituto Nazionale di Astrofisica, Istituto di Radioastronomia, Via Piero Gobetti 101, 40127 Bologna, Italy.
[2]. University of Southern Queensland, Centre for Astrophysics, West St, Darling Heights QLD 4350, Australia.
[3]. Università degli Studi Roma Tre, Dipartimento di Matematica e Fisica, Via della Vasca Navale 84, 00146 Rome, Italy.
[4]. Istituto Nazionale di Astrofisica, Istituto di Astrofisica e Planetologia Spaziali, Via del Fosso del Cavaliere, 100, 00133 Roma, Italy.
[5]. Centro euro-Mediterraneo sui Cambiamenti Climatici, Divisione Ocean Predictions and Applications, Via Marco Biagi 5, 73100 Lecce, Italy.
[6]. Università del Salento, Dipartimento di Matematica e Fisica "Ennio de Giorgi", Via Provinciale per Arnesano, 73100 Lecce, Italy.
[7]. Istituto Nazionale Fisica Nucleare, Sezione di Lecce, Via Provinciale per Arnesano, 73100 Lecce, Italy.
[8]. Enginium S.r.l., Via Luigi Cadorna 67, 20090 Vimodrone, Italy.
[9]. Consiglio Nazionale delle Ricerche, Istituto per il Rilevamento Elettromagnetico dell'Ambiente, Via Diocleziano 328, 80124 Naples, Italy.

* Corresponding author: Graziella.Caprarelli@usq.edu.au

Abstract

The principal objective of the radar sounder MARSIS experiment is to look for ice and water in the Martian subsurface. One particular focus of investigations, since 2005, has been the search for basal liquid water in the south polar layered deposits (SPLD). Anomalously strong basal echoes detected from four distinct areas at the base of the deposits at Ultimi Scopuli have been interpreted to indicate the presence of bodies of liquid water in this location, beneath a 1.5 km thick cover of ice and dust. Other explanations for the bright basal reflections have been proposed, however, including the possibility of constructive interference in layered media. Here, we test this mechanism through simulations of MARSIS radar signals propagating in models of CO_2-H_2O ice sequences. We then compare the results to real MARSIS data acquired over Ultimi Scopuli, finding that no CO_2-H_2O ice model sequence reproduces the set of real data. The results of our work have implications in relation to the global CO_2 inventory of Mars.

Keywords: Mars, SPLD, MARSIS, CO_2 ice, radar.

1. Introduction

The radar sounder MARSIS (Mars Advanced Radar for Subsurface and Ionospheric Sounding) on board the European Space Agency orbiter Mars Express, has been probing the Martian subsurface since 2005 (Orosei et al., 2015), exploring the global distribution of rock, soil, ice, and liquid water. The instrument operates within the range 1.3-5.5 MHz, transmitting a 1 MHz-bandwidth pulse centered at the frequencies of 1.8, 3, 4 and 5 MHz. Exploration of the Martian subsurface is mostly carried out using the 3 and 4 MHz, or 4 and 5 MHz frequencies, for a nominal depth of investigation of up to 5 km, depending on the electromagnetic properties of the probed material (Picardi et al., 2004).

The primary objective for the MARSIS experiment is to look for buried ice and water in the Martian subsurface. It was not until 2018, however, that evidence of bright subsurface reflections originating 1.5 km deep below the surface of Ultimi Scopuli, one of the terminal regions of the South Polar Layered Deposits (SPLD), was obtained (Orosei et al., 2018a) at coordinates 193°E - 81°S. The reflections, much brighter than those detected from the surface, were interpreted as originating from basal ponded water or wet sediments distributed on an area approximately 20 km across. The work reignited the scientific debate about the stability of liquid water at the Martian polar regions, and specifically at the south pole, where average surface temperatures (Mellon et al., 2004) are estimated to be 162 K. A possible explanation for the water being liquid at these conditions is that it contains a high concentration of salts (e.g., perchlorates, chlorides) which are ubiquitous on Mars (Hecht et al., 2009) and have eutectic temperatures as low as 198 K (Pestova et al., 2005). It was subsequently suggested that a high geothermal gradient, such as that produced by a magmatic chamber at depth, is required to reach the eutectic temperatures of concentrated salt solutions at the base of the deposits (Sori and Bramson, 2019). This scenario was disputed, however, on the grounds that there is no evidence of an anomalous geothermal gradient in the region (Lauro et al., 2021). Newly acquired MARSIS orbits of the region further revealed other three previously undetected areas of bright reflections, each approximately 10 km across (Lauro et al., 2021). Because laboratory experiments have shown that hypersaline aqueous solutions can form and persist over time at temperatures as low as 123 K, well below their eutectic temperatures (Toner et al., 2014; Primm et al., 2017), a hypersaline origin of the water was deemed to remain the most likely explanation for the bright reflections (Lauro et al., 2021). It is however difficult to envisage how large bodies of supercooled brines could have persisted in the natural Martian environment over geological timescales (Schroeder and Steinbrügge, 2021; Smith et al., 2021), which remains a significant argument against the liquid brine interpretation. The possibility that bright reflections could be caused by scattering phenomena in a stratified medium was also raised (Hecht et al., 2018). This criticism was however dismissed by Orosei et al. (2018b), who pointed out that they had demonstrated that the strength of the basal echoes at Ultimi Scopuli cannot be explained by multiple reflections. Even though a particular stratigraphic arrangement could produce enhanced basal echoes at one of the MARSIS frequencies of detection, it did not do so at the other observation frequencies. Alternative models suggesting that a range of materials, other than bodies of liquid water, could explain the sources of the strong basal echoes, have recently been published by Bierson et al. (2021), and Smith et al. (2021). The merits of all proposed alternative hypotheses have been reviewed by Schroeder and Steinbrügge (2021), who argued that none of the alternatives is conclusively incompatible with bodies of liquid water as the source of the bright basal reflections, and that each model opens up questions providing new opportunities for future investigations.

Distinct layers of CO_2 ice have been detected by radar sounder SHARAD surveys of the SPLD (Phillips et al., 2011; Bierson et al., 2016). The layers, up to 1 km thick, are interlayered with thin (typically 10-40 m thick) water ice, and it has been calculated that sublimation of these massive deposits of CO_2 ice would increase the Martian atmospheric pressure by 100% (Bierson et al., 2016). It has been suggested that, if the conditions leading to formation of the thick CO_2-H_2O ice deposits have occurred at other times, during the approximately 100 Myr history of formation of the SPLD (Manning et al., 2019), then a specific CO_2 ice layering configuration might produce subsurface reflections of higher intensity than those from the surface. In fact, Lalich et al. (2021a,b) obtained strong simulated radar reflections at 4 MHz frequency, mimicking MARSIS waveform, for a model configuration involving 1-100 m thick basal CO_2 ice layers sandwiching a dusty water ice layer of comparable thickness. Such configuration over the extent of MARSIS bright area, would translate in an average ~ 2% of the current CO_2 atmospheric content. While this specific contribution to the atmospheric volatile budget appears negligible, compounding scenarios involving storage of volatiles within the south polar cap can potentially impact estimates of the Martian volatile budget, with consequences on models of Martian climate cycles and atmospheric evolution, and on estimates of the amount of volatiles stored in the Martian crust as part of the geological record.

The Martian polar caps are the most voluminous exposed reservoirs of volatiles on Mars. It is estimated that, combined, the polar caps store two thirds of the entire water content of the planet (Catling, 2014; Smith et al., 2020; Jakoski, 2021). While climate models have suggested the possibility that the polar layered deposits may also contain significant amounts of CO_2 (Jakoski et al., 1995), estimates based on thermophysical properties of water and CO_2 ices rejected such interpretation (Mellon, 1996). The thin veneer of seasonal and residual solid CO_2 on the surface of the polar caps is effectively counted as part of the atmosphere (Jakosky, 2019). However, geomorphological (Gulick and Baker, 1989; Baker et al., 1991; Baker, 2001; Ramirez and Craddock, 2018) and geochemical evidence (Bridges et al., 2019) has been interpreted to indicate that early Mars was warmer and wetter than at present, prompting suggestions that a thick CO_2 rich atmosphere existed at the time, to account for greenhouse heating of the planet (Haberle et al., 1994). It has been argued that subsequent loss to space of the CO_2 (and other volatiles) does not fully account for the present-day content of CO_2 in the current thin Martian atmosphere, and that massive quantities of CO_2 ought to be sequestered within one or more geological sinks on Mars (Forget et al., 2013). While deep-seated carbonates could in principle accommodate large volumes of CO_2 (Kahn, 1985; Michalski and Niles, 2010; Wray et al., 2016; Jakosky, 2019), as is the case on Earth, there is at present no conclusive evidence for a global deep-crustal reservoir of carbonates on Mars (Edwards and Ehlmann, 2015). The discovery of massive deposits of CO_2 ice (Phillips et al., 2011; Bierson et al., 2016) in the South Polar Layered Deposits (SPLD) by the radar sounder SHARAD, and three-dimensional radar imaging volume calculations suggesting the deposits may contain more than $1.6 \cdot 10^4$ km^3 of dry ice (Putzig et al., 2018), have thus paved the way for renewed investigations into the possibility of the polar ice caps as CO_2 sinks.

The global abundance of CO_2 on Mars is presently unknown. There are some generally accepted points, however, that hold irrespective of the exact abundance and distribution of CO_2 on Mars. Mars had lost most of its CO_2 rich atmosphere by the end of the Noachian (~ 3.7 Ga) (Jakosky, 2019). The rate of input of juvenile gases into the atmosphere through planetary outgassing (i.e., volcanic activity) is not known precisely, but it was higher during the Noachian, waning in the Hesperian, becoming negligible in the Amazonian (Grott et al., 2011), so it would have been insufficient to replenish the lost early atmospheric budget. It is not known how much of the initial Martian atmosphere was left by the end of the Noachian (estimates range from ~ 0.1 bar to 1 bar; Catling, 2014), and how much CO_2 had by then already been stored in crustal sinks, though it is clear that the overall trend since has been one of thinning of the atmosphere to the present-day global value of ~ 6 mbar of pressure. If the massive CO_2 ice deposits (Phillips et al., 2011) were to sublimate, they would add to the atmosphere as much as ~0.006 bar of CO_2 (Bierson et al., 2016). Further compounding the contribution (however small) of putative additional reservoirs of CO_2 ice hidden in the SPLD, could potentially impact estimates of the planetary CO_2 budget.

Here, we present the results of our comprehensive testing of model simulations against the database of MARSIS data acquired over more than 10 years of surveys of the south polar region. We modeled the propagation behaviour of electromagnetic waves at MARSIS operating frequencies (1.8-5 MHz) under a variety of conditions involving different configurations of thin layers of solid CO_2, H_2O ice and dust. Within the parameter space we explored, the models do not return values of reflection consistent with the observed MARSIS data. We thus reject the notion that the bright basal reflections detected at Ultimi Scopuli may indicate the presence of thin layers of CO_2-ice at the base of the SPLD.

2. Geological Setting

The South Polar Layered Deposits (SPLD), covering most of the Planum Australe of Mars (Fig. 1), form an up to 3.7 km thick (Plaut et al., 2007) stratified unit, composed of pure water ice interlayered with thin dust-rich deposits. It has been estimated that the content of dust in the SPLD is ~ 10-15% (Plaut et al., 2007; Zuber et al., 2007), although inhomogeneities in the values of inverted density of the deposits indicate that the dust is not uniformly distributed (Li et al., 2012), and that the fraction of dust in the water ice would vary depending on the presence of denser CO_2 ice (Broquet et al., 2021). The layers are directly observed in radar imagery where troughs and scarps cut through the deposits (Milkovich and Plaut, 2008). Owing to the electromagnetic contrast between the values of dielectric permittivity ε of ice (3.12; Pettinelli et al., 2015) and dust (> 4; Mattei et al., 2014), layering is also detected by radar sounder observations (Plaut et al., 2006, 2007; Milkovich et al., 2009; Whitten and Campbell, 2018). Layering of the deposits is thought to reflect differential dust and ice accumulation rates influenced by global climate cycles linked to orbital forcing (e.g., Hvidberg et al., 2012). The deposits decrease in elevation and thickness at the margins, eventually waning and revealing underlying Noachian and Hesperian highlands terrains (Tanaka and Kolb, 2001), overlain by a thin mantle of desiccated or water-ice pore-filled soil (Putzig et al., 2005; Jones et al., 2014). The surface age of the SPLD is 7-100 Ma, based on the impact crater record (Herkenhoff and Plaut, 2000; Koutnik et al., 2002). The age of the lowermost strata of the SPLD sequence is presently undetermined. A detailed geological analysis and interpretation of the unconformities observed in Promethei Lingula suggests that the current extent of the SPLD may have started forming no earlier than 250 Ma (Guallini et al., 2018). This estimate is consistent with time-series analysis of HiRISE and CaSSIS stereo-images of the internal structure of the SPLD shown along scarp faces, suggesting that the minimum time of accumulation of the SPLD is 10-30 Myr, resulting in a minimum age of deposition for the basal layers of 17 to 130 Ma (Becerra et al., 2019).

The SPLD have been subdivided into three distinct structures (Milkovich and Plaut, 2008): the *Promethei Lingula Layer* Sequence (PLL), the *Bench Forming Layer* Sequence (BFL), and the *Inferred Layer* Sequence (IL). The BFL is the top sequence, geographically located in the central west-northwest portion of the SPLD, where the deposits measure their highest elevations (~ 3500-4500 m). The BFL is covered by thin layers of CO_2 ice (part of the South Polar Residual Cap, SPRC). Underlying the BFL is the PLL, while IL is inferred to be the basal sequence in the west of the deposits. Elsewhere, only the PLL exists (ref. to figs. 18-19, in Milkovich and Plaut, 2008), its lateral extent corresponding to that of Tanaka et al.'s (2014) *Apu* (Amazonian polar undivided) unit (Fig. 1).

The South Polar Residual Cap (SPRC), which is part of geological unit *lApc* (Fig. 1), straddles the prime meridian, approximately between longitudes 250°E-40°E and latitudes 85-90°S. The cap is primarily composed of a high albedo thin (<10 m) layer of CO_2 ice (Byrne and Ingersoll, 2003), with a characteristic «Swiss cheese» appearance (Malin et al., 2001) due to the presence of pits that reveal underlying water ice (Zuber et al., 2007). Observed constant rates of erosion of the pits (Thomas et al., 2013) have been interpreted to point to net loss of CO_2 from the SPRC, possibly counterbalanced by observed net gain of seasonal water ice (Brown et al., 2014), suggesting orbital effects are responsible for the CO_2 and H_2O atmosphere-SPRC exchanges. Localized deposits up to 1 km thick, formed by alternating layers of CO_2 ice (each approximately 100 m thick) and H_2O ice (a few m thick) have also been detected (Phillips et al., 2011; Bierson et al., 2016) by the radar sounder SHARAD, in troughs and at the base of scarps of the BFL structural unit, to the west of the location of the inferred rim of the ~ 870 km diameter Noachian impact crater Prometheus Basin (Fig. 1). This suggests a possible relationship between the basal topography in this area, and atmospheric conditions that caused deposition of CO_2 ice here. It has been proposed that H_2O ice entombs the CO_2 ice layers, thus isolating them from the atmosphere and preventing their erosion (Manning et al., 2019). An alternative hypothesis argues that the deposits are in communication with the atmosphere, and that variations in polar incident sunlight from Mars's 100 kyr orbital cycles balance the exchange between CO_2 in the deposits and in the atmosphere. The observed deposits should thus record the last 510 kyr of Martian polar climate history (Buhler et al., 2021). Observations by SHARAD and MARSIS radars did not detect CO_2 ice layers anywhere else in the SPLD (Whitten et al., 2017; Whitten and Campbell, 2018; Khuller and Plaut, 2021).

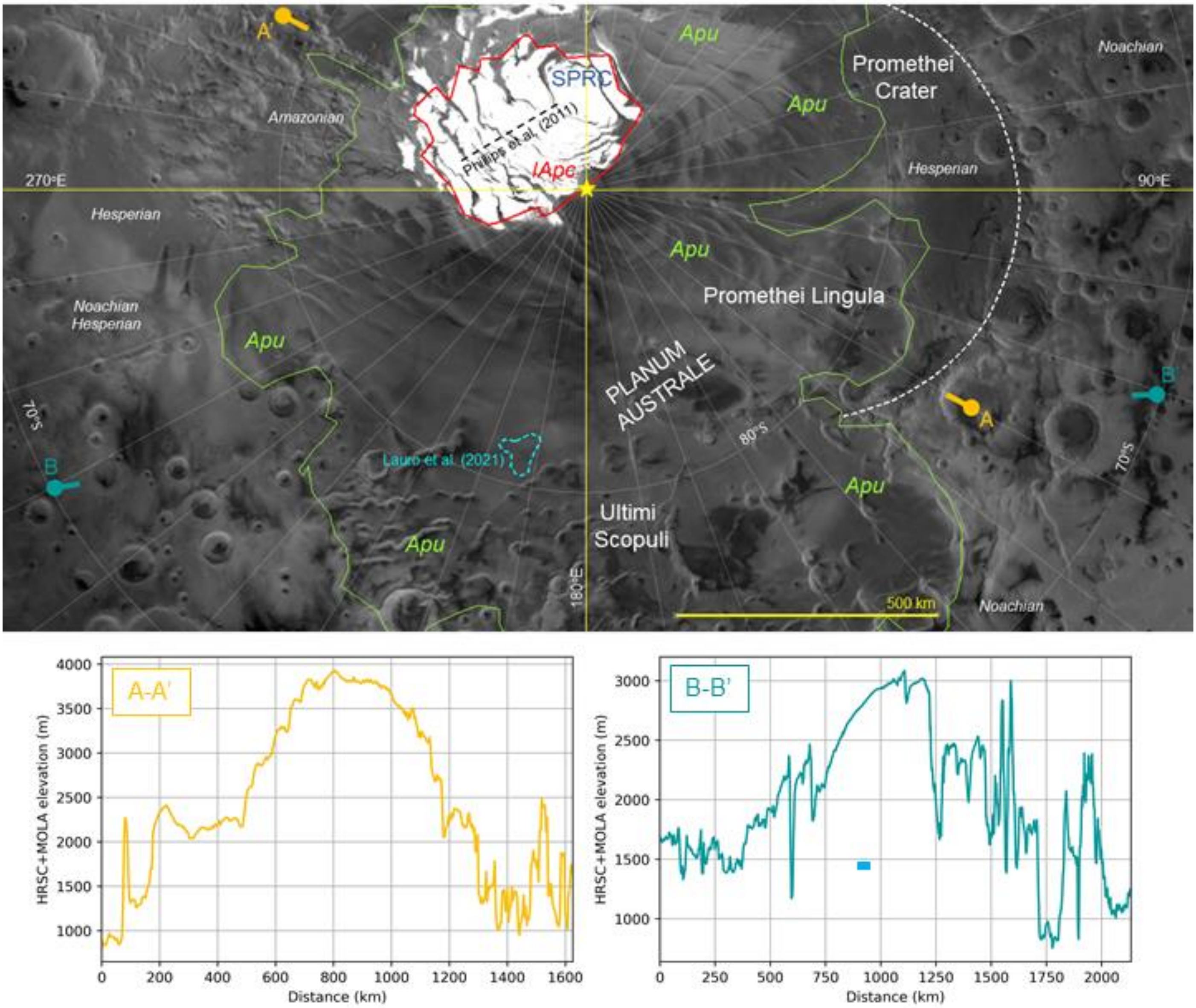

Fig. 1. Context map of the south polar region. The map shows the extent of the geological units and geographic features described in Section 2. The dashed aqua polyline indicates the location of the strong basal reflections detected by Lauro et al. (2021). The trace of the ground track of the tract of SHARAD orbit 5968-01 traversing the RFZ_3 (Phillips et al., 2011) is shown as a black dashed line on the south pole residual cap (SPRC). Yellow star: South Pole. Vertical yellow line: prime and anti- meridians. Dashed white line: approximate position of remnant of rim of Promethei Crater. Lime green polyline: boundary of Amazonian polar undivided unit (*Apu*). Red polyline: boundary of late Amazonian polar cap unit (*lApc*). A-A': end points of topographic profile A-A' (orange). B-B': end points of topographic profile B-B' (green). The short light blue segment in topographic profile B-B' indicates the

position and inferred depth of the bright basal reflections. Elevations are blended DEM/DTM (200 m/pixel) from MOLA and HRSC data. Geological units are described by Tanaka et al. (2014). Geographic grid interval: 10°. Mapped with JMARS.

Ultimi Scopuli is a vast terminal region of the deposits, part of the *Apu* geological unit (Fig. 1) and of the structural PLL sequence. Here, between coordinates 191°E-196°E and 80.3-81.5°S, and at a depth of approximately 1.5 km, recent orbiter sounder MARSIS observations (Orosei et al., 2018a; Lauro et al., 2021) revealed the presence of four high permittivity areas, interpreted to be bodies of basal liquid water. The heat flow at the Martian south polar regions is ~ 22-26 mW/m^2 (Grott et al., 2013; Plesa et al., 2018), and there is presently no evidence of an anomalous geothermal gradient or localized hot spot (such as a magma chamber, as postulated by Sori and Bramson, 2019), that would plausibly increase the basal temperature. The overburden pressure, estimated to be ~ 6 MPa (considering an average density of the SPLD = 1220 kg/m^3, from Zuber et al., 2007, which is the same as the best fit value published by Broquet et al., 2021, and also consistent with a local value of ~ 1200 kg/m^3, as inferred from the inverted density map of the SPLD published by Li et al., 2012), would also be insufficient for ice to melt. Therefore, to explain the presence of basal liquid water, Orosei et al. (2018a) suggested that the water may be a perchlorate brine. Subsequently, Lauro et al. (2021) further defended this interpretation, on the grounds that supercooled perchlorate brines have been shown to form and persist at sub-eutectic temperatures (Toner et al., 2014; Primm et al., 2017), within the range of those reasonably expected at the base of the SPLD. The reflections at the base of Ultimi Scopuli are located over a gently sloping basement (Lauro et al., 2021).

3. Model

3.1. Preliminary Analysis

The fundamental concept underpinning this study is that the electromagnetic waves locally reflected from interfaces between the layers in a stratified structure, can combine to enhance (constructive interference) or suppress (destructive interference) the overall radar response from a layered structure. As a preliminary analysis, we explored the specific parameter space presented by Lalich et al.'s (2021a) model, consisting of a thin layer of pure water ice sandwiched between two thin layers of CO_2 ice: thus, we modelled the variation of only three parameters, i.e., the thickness of each of the three layers. Layer thicknesses greater than a few tens of m dampen resonance effects, because longer propagation paths decrease the likelihood of simultaneous in-phase sum of sinusoids at different frequencies (Supplementary Figure 5, Orosei et al., 2018a). Therefore, we constrained the simulated thickness of each layer to be $\leq$ 100 m. In the field of numerical electromagnetic modelling, spatial discretization is usually set to be less than 1/10 of the wavelength. The shortest wavelength transmitted by MARSIS is 30 m in water ice. Thus, we applied simulated thickness increments of 1 m as our sampling interval, to obtain accurate model stratigraphy responses to the MARSIS pulses. We ran more than one million simulations (101 × 101 × 101) at MARSIS operating frequencies of 3, 4 and 5 MHz, obtaining a complete characterization of the properties of Lalich et al.'s (2021a) model.

The highest value of subsurface-to-surface echo power ratio we obtained was 4.7 dB. Because the radar response to the stratigraphy is described by sinusoidal functions, we ruled out the eventuality that we might have missed peaks in the subsurface echo: considering that variations in the radar response between consecutive data points are negligible (a fraction of a decibel at most), the model stratigraphy subsurface-to-surface echo power ratios would never exceed ~ 5 dB, even in the case that the position of our maxima were not exact.

For each frequency, we obtained five well-defined regions in parameter space with subsurface-to-surface radar echo power ratio values > 4 dB (Fig. 2). These regions are specific to each frequency, because constructive interference phenomena are primarily controlled by layer thickness / wavelength ratios. Consequently, while basal echo powers remain high for small variations of thickness around the local maxima at one frequency, the corresponding echo powers at the other two frequencies are lower and much more widely dispersed (Fig. 3). Thus, if we take the parameter values corresponding to the maxima found at one frequency as a reference, and calculate the subsurface-to-surface echo power ratio differences between this frequency and the other two, these will always favour the reference frequency (Fig. 4).

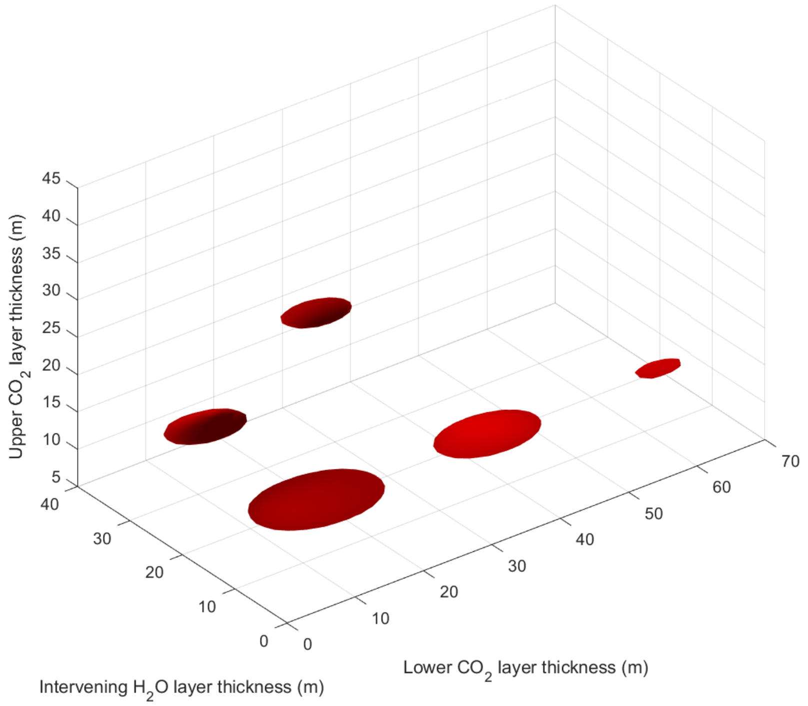

Fig. 2. Location of strong basal echoes (> 4 dB greater than surface echoes) produced in simulations at 4 MHz, displayed in the parameter space of the model by Lalich et al. (2021a), consisting of three quantities, specifically: the thickness of two CO_2 layers, and of a pure water ice layer sandwiched between them. Simulations at 3 and 5 MHz produce the same pattern, but with local maxima in different positions.

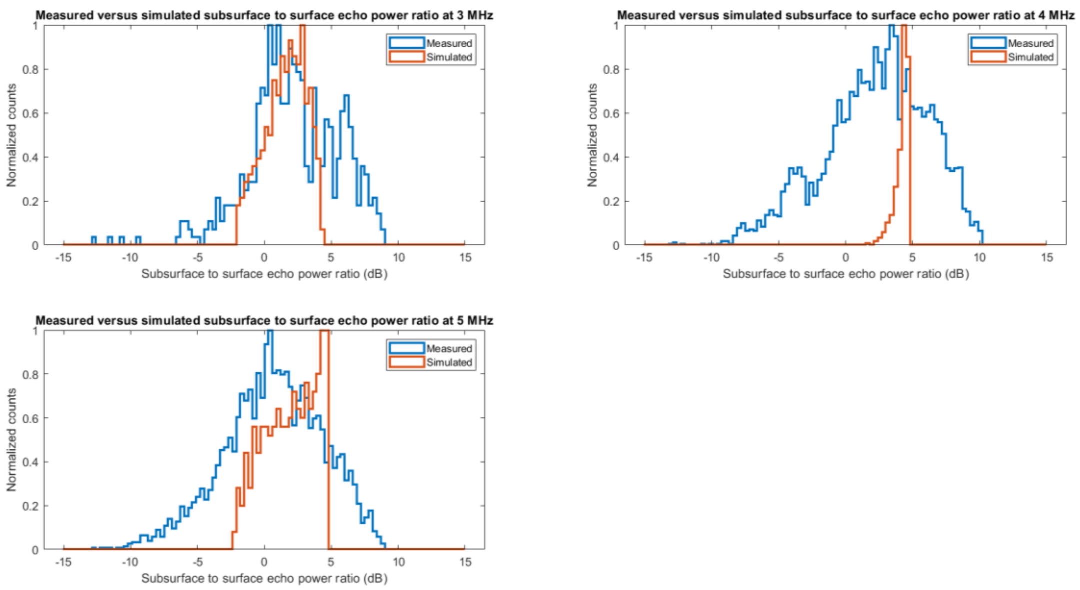

Fig. 3. Histograms of subsurface-to-surface echo power ratios obtained for simulations (orange) with a bottom CO_2 ice layer of thickness ranging between 8 m and 14 m, a top CO_2 ice layer 9-15 m thick, and an interbedded H_2O ice layer 9-15 m thick. Blue histograms represent real MARSIS observations.

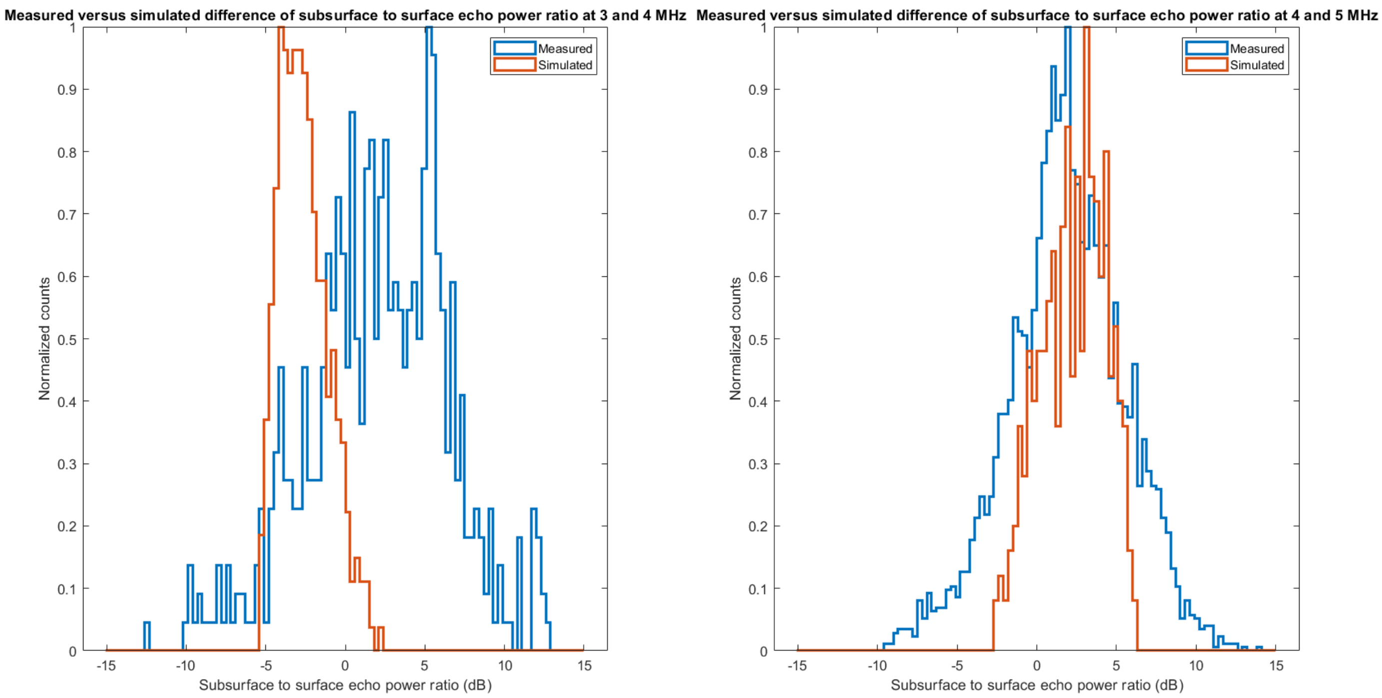

Fig. 4. Histograms of basal-to-surface echo power ratio differences between pairs of MARSIS operating frequencies (3 and 4 MHz, and 4 and 5 MHz). Simulation conditions are the same as for those in Fig. 3. Blue histograms are for real MARSIS observations.

Our preliminary analysis indicates that the distribution and behavior of subsurface-to-surface echo power ratios simulated in the parameter space as described, contrast sharply with that of real MARSIS data. However, idealized models do not consider possible sources of echo power fluctuations that affect real data, and thus some discussion is needed before a comparison between data and model is attempted.

The model used and discussed by Orosei et al. (2018) is computationally the same used by Lalich et al. (2021a, 2021b), that is the one-dimensional solution of Maxwell equations in a plane parallel stratigraphy. The former model had a simpler stratigraphy compared to the latter, with the SPLD represented as a single homogeneous layer composed of a mixture of H_2O ice and dust. The model was run varying basal temperature, dust content and basal permittivity. These three parameters controlled the attenuation within the SPLD and the intensity of the reflection at the bottom of the SPLD. The results showed that even for low amounts of dust and basal temperatures, it was necessary to have a high basal reflectivity to produce the observed strong basal echoes.

The model parameters published by Lalich et al. (2021b) are exactly the same, except for the input of single values for dust fraction, basal temperature and basal permittivity. These authors varied the thickness of the layers at the base of the SPLD.

Because of the similarity of the mathematical formulation of the two models, we compared them directly to one another to assess their capability to reproduce MARSIS observations, following the same approach used by Lalich et al. (2021b). For example, Figure 3 in that paper shows reflections produced by a single CO_2 layer model that are as strong as the ones observed by MARSIS, although the authors neglected to specify that their reference values for MARSIS echo power are the medians of observed values, and that normalized echo power can reach values as high as 10 dB (see Figure 4 and S4 in Orosei et al., 2018), well above any value that can be obtained by the single layer model shown in Figure 3.

The capability of the model in Orosei et al. (2018) to produce strong echoes is thus not due to a more complex mathematical implementation or to a greater number of parameters, but to the fact that basal permittivity can have higher values than those considered by Lalich et al. (2021a, 2021b). In fact, Orosei et al.’s (2018) model could produce basal echoes spanning the full range of observed values (see their Figures 4 and S4), whereas Lalich et al.’s (2021a, 2021b) resulted only in a few instances of basal echo power comparable to observations. The purpose of the present work is therefore to establish the conditions (if these exist), by which Lalich et al.’s (2021) model reproduces the strong radar echoes reported by Orosei et al. (2018). We thus performed comprehensive simulations based on the same mathematics, using a range of possible parameters beyond that explored in that earlier work.

In the following sections, we discuss the sources of variability and error affecting MARSIS observations, evaluating their effect to derive a model of the uncertainties that can be applied to model results, for a more realistic comparison between simulations and data.

3.2 Idealized vs. actual SPLD surface geometry

The assumption of a perfectly flat surface does not prevent the possibility of a comparison with real data, as already shown by Orosei et al. (2018). Furthermore, the subsurface echo power for a given orbit is always normalized to its median value, in order to prevent local minima of surface echo power from producing unrealistically high normalized subsurface echo power values. The choice of using surface median power implies the assumption that the SPLD surface is locally homogeneous, and that surface echo power fluctuations are due to small perturbations of this assumed homogeneity.

To verify if this assumption holds, we need to examine the properties of echo power measured by MARSIS. To this end, we retrieved the same data employed to produce Figure 2 in Orosei et al. (2018) and made publicly available at the time of publication of that paper (Orosei and Cicchetti, 2018). We also produced a simulation of surface echo power similar to those presented and discussed in Orosei et al. (2015). Simulations are used to validate subsurface echo detection by visual comparison: all features present in both the real and simulated radargrams are interpreted as surface clutter, and are therefore excluded from interpretation. A comparison between measurements and simulations for orbit 10737 is shown in Figure 5.

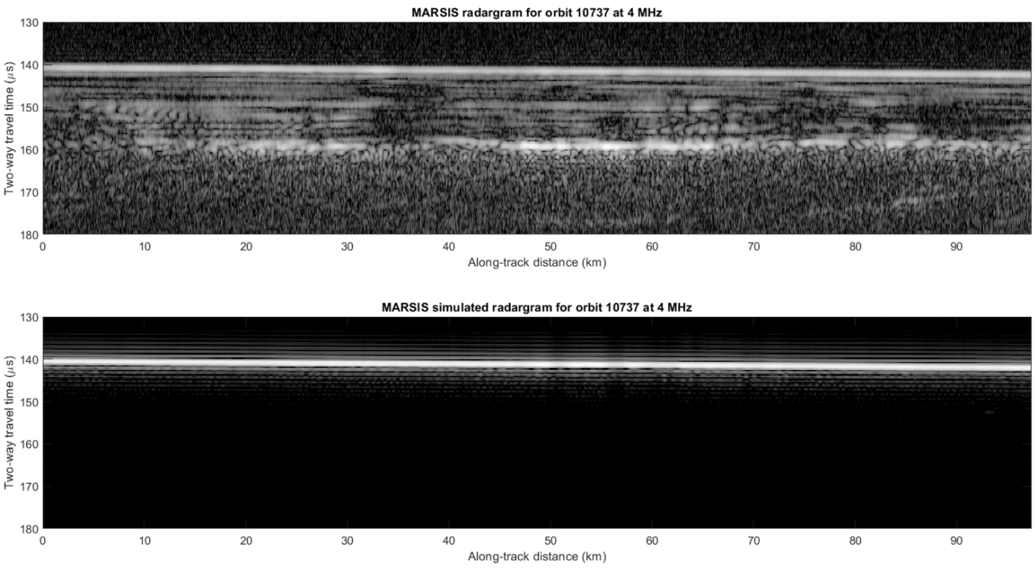

Fig. 5. Top: MARSIS radargram for orbit 10737 at 4 MHz, redrawn following Orosei et al. (2018), versus the corresponding simulation of surface scattering produced using the MOLA topographic dataset (bottom).

The simulated radargram allows also to estimate surface power fluctuations due to surface roughness alone, sampled at the resolution of the MOLA topographic dataset. A comparison with the measured surface power (both arbitrarily normalized to a 0 dB median power for ease of comparison) is shown in Figure 6: it is clear that surface roughness alone accounts for the surface echo power fluctuations at distances between 50 and 60 km along track, which correspond to the location of the bright subsurface reflector.

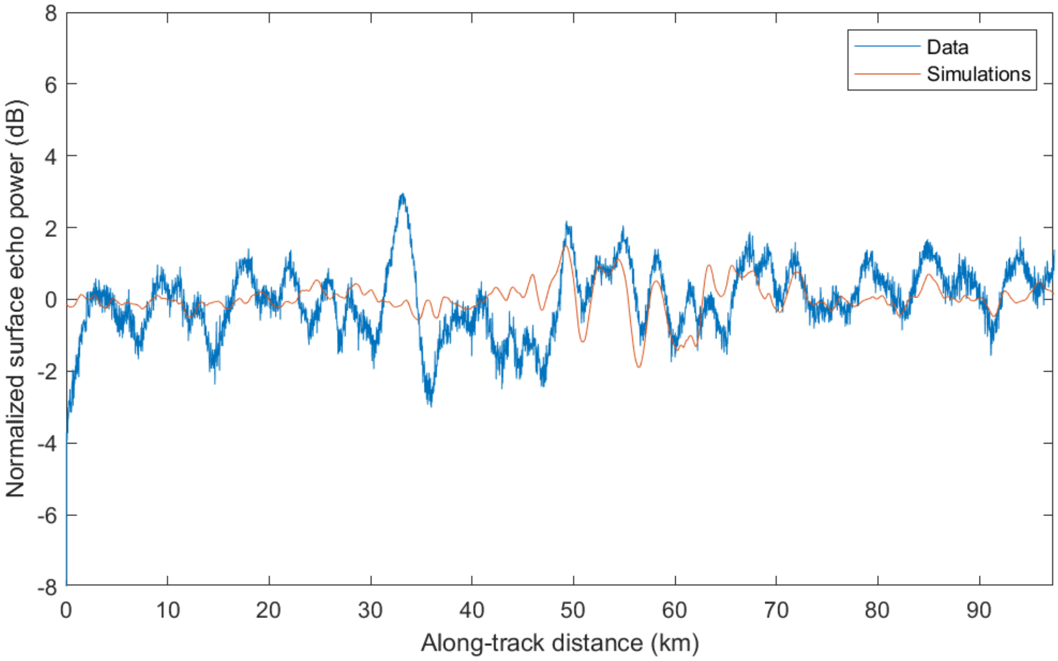

Fig. 6. Measured vs. simulated surface echo power for orbit 10737 at 4 MHz, both arbitrarily normalized to a 0 dB median power for ease of comparison.

The residual difference between data and simulations can be attributed to several factors, such as: surface roughness at scales below MOLA resolution or variations in near-surface density and composition, but the exact cause is difficult to ascertain with available data. Residual power fluctuations are found to have a standard deviation of less than 1 dB, corresponding to a fluctuation of 0.5 in the value of the relative dielectric constant in the assumption that its median value is comprised between 3 and 4 (typical of SPLD materials). Because of the small uncertainties resulting from this analysis, we consider the ratioing with the median surface power as a reasonable calibration method for subsurface echo power.

Furthermore, a previous analysis of SHARAD echoes by Grima et al. (2012) over this area (called Reference Zone or RZ in the paper because of its flatness) showed that surface reflections are predominantly coherent, implying that scattering is near-specular and thus approximates that of a plane surface. This conclusion is even truer at MARSIS wavelength, as the effect of roughness on scattering does not depend on RMS topographic height, but rather on the ratio between RMS topographic height and the wavelength.

It could be argued that even a small roughness causes a decrease (however small) of the mean power of surface echoes, leading to an overestimation of the subsurface-to-surface echo power ratio. In fact, the opposite is true: electromagnetic models and three-dimensional propagation simulations (e.g., Jonard et al., 2019) demonstrate that the wavefront of the radar pulse penetrating through the subsurface is disrupted more than the echo backscattered at the surface, because it crosses the rough surface twice. Thus, the subsurface to surface echo power ratio calculated assuming no surface roughness effect, should be considered a minimum value, with the real ratio likely higher.

3.3 Signal distortion and noise

The MARSIS pulse is not an ideal chirp. Its actual shape and power are unknown: in fact, the spectra reported by Jordan et al. (2009) do not include the frequency-dependent effects of antenna gain, because these could not be measured on ground owing to the length of the antenna. A test comparing the results obtained using Jordan et al.'s (2009) chirp spectra with those obtained using the ideal chirp, does not demonstrate any significant difference. Therefore, the MARSIS data have been range-compressed using an ideal chirp since the beginning of the mission. The range compression is not optimal, with both resolution and signal-to-noise ratio affected. This, however, does not affect the ratio of subsurface to surface echo power. In an abstract mathematical representation, radar sounding can be described as the convolution of the radar waveform with the ideal electromagnetic response of the observed scene. In Fourier transform terms, this convolution is the multiplication of the stratigraphy spectral response with a band-limited signal spectrum, which clips the spectral response bandwidth and produces a limited resolution time-domain response. All these mathematical operations are linear, so the shape of the pulse spectrum will change the power level of echoes from two different interfaces, but not their ratio, which is the quantity used in this analysis.

A few available data also point to a possible dependence of gain on temperature, although a full characterization of this effect was never performed, because it was considered to be negligible under the conditions at which MARSIS acquires its observations. Furthermore, MARSIS raw data takes are at most 25 seconds long, which is too short a time to produce any significant gain variation. This is further corroborated by the plot of surface echo power shown in Figure 6, which does not show any trend of varying gain across the entire observation. Thus, within the limits of what it is technically possible to ascertain about the causes and extent of non-ideality of range compression in MARSIS, there is no effect that should be considered as introducing a bias in the use of median surface echo power as a calibration reference for subsurface echo power.

Plots of the noise level in the observations (Orosei and Cicchetti, 2018) analysed by Orosei et al. (2018) show constant noise level across a single observation, and nearly-constant noise levels across observations at the same frequency (around -5 dB at 3 and 4 MHz and -11 dB at 5 MHz when expressed in uncalibrated digital numbers). The median signal-to-noise ratio is > 20 dB for all observations, exceeding 30 dB.

Interferences caused by the electronics of the Mars Express spacecraft were characterized in the commissioning phase of MARSIS. Limited available documentation shows a correlation with the activity of the HRSC camera, though no systematic analysis has ever been published. Overall, data acquired over the lifetime of the mission show that the combined electromagnetic interferences (EMI) caused by orbiter navigation and experiment instrumentations, have a much smaller effect on the functioning of MARSIS than (for example) on its Mars Reconnaissance Orbiter companion SHARAD. Thus, the operating assumption is that EMI have a negligible effect on the subsurface to surface echo power ratio.

The MARSIS data analyzed by Orosei et al. (2018) consist of near-simultaneous observations at two frequencies, namely 3 and 4 MHz, or 4 and 5 MHz. Thus, it is possible to compute the subsurface to surface echo power ratio at two frequencies for the same observation. Doing so for data in which surface echo power has a standard deviation below 1 dB (as noted in Table S1 in the Supplementary Materials of Orosei et al., 2018), one is left only with data at 4 and 5 MHz. The difference between normalized power at those two frequencies has a median value of 1.36 dB, which can be used for a back-of the envelope computation based on equations found in Porcello et al. (1974) to obtain an estimate of the loss tangent (see also Orosei et al., 2020 for the effect of such loss tangent value on SHARAD measurements). The resulting value is approximately 0.03, which is about fifteen times greater than the one used by Lalich et al. (2021b). Because this value is affected by a large error (the standard deviation of the difference between normalized power at the two frequencies is almost 4 dB), we did not use the estimated loss tangent in simulations. Instead, we considered a variable attenuation as one of the factors decreasing the measured ratio between subsurface and surface power produced by a model.

3.4 Other factors affecting subsurface to surface echo power ratio

Factors affecting subsurface echo power not included in Orosei et al.'s (2018) models are: surface roughness (as discussed above); subsurface roughness (affecting basal echo intensity only); fraction of the radar footprint covered by the basal reflector (see for example Haynes et al., 2018, for a discussion); signal attenuation within the SPLD due to dielectric losses (as discussed above); signal attenuation within the SPLD due to reflection losses in the thinly layered stratigraphy (see for example Courville et al., 2021, for a detailed modelling of propagation in a layered medium at SHARAD frequencies). Their combined effect is demonstrated by the large dispersion of values observed (Figure 7).

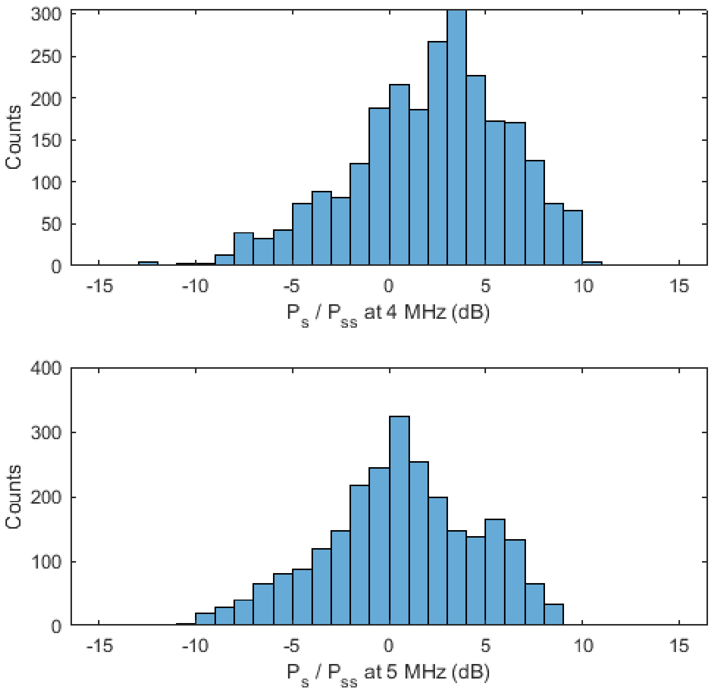

Fig. 7. Histograms of measured values of subsurface to surface echo power ratio over the bright reflector analysed in Orosei et al. (2018) at 4 MHz (top) and 5 MHz (bottom).

The histograms are asymmetric, with a cut-off at high values and a long tail towards low ones. This characteristic matches the intuitive notion that the intensity of a basal reflection cannot increase indefinitely, and would thus have a maximum possible value obtained when all the factors contributing to decreasing basal echo intensity as discussed above are minimized. Thus, a comparison between simulations and data requires the introduction of a model for the random dispersion of measurements. As it is not possible to quantify separately the importance of each factor contributing to basal echo power attenuation, we derived a model probability density function directly from the data (Fig. 8).

The long left-sided tails of the histograms in Figure 7 are characteristic of generalized extreme value distributions, often used to model the maxima of sequences of random variables. Although this is a heuristic method for the selection of the model distribution, it has the merit of matching data histograms better than other parametric distributions.

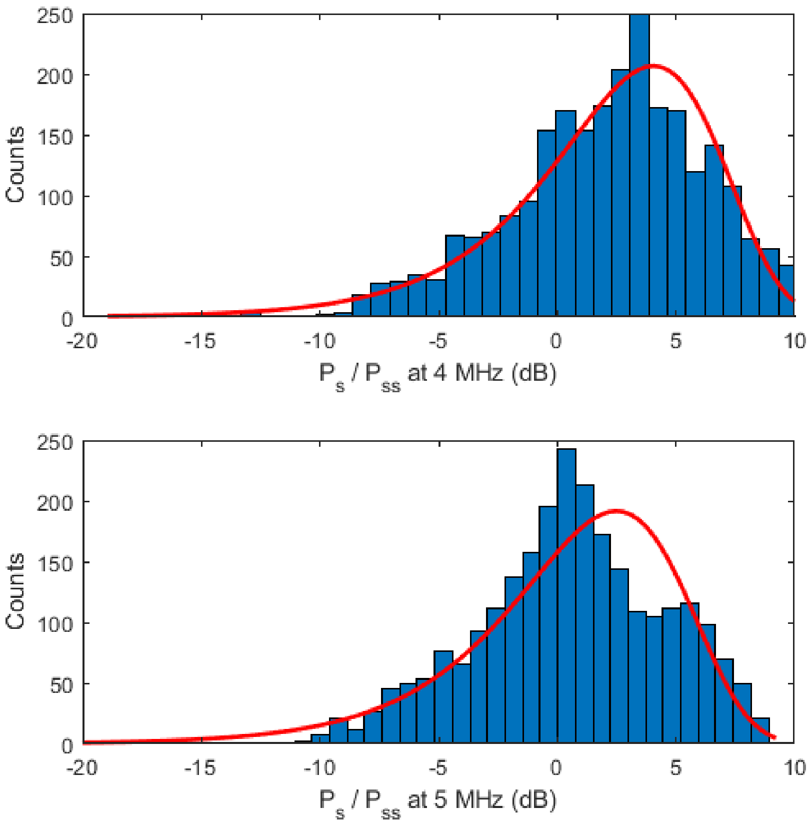

Fig. 8. Best-fit extreme value distributions plotted over the histograms shown in Figure 7.

Through the remainder of this paper, we use these best-fit distributions as the template for randomly generating synthetic measurements from models.

3.5. Electromagnetic propagation model

The propagation of radar waves across stratified media is described by non-linear equations dependent on the electromagnetic properties and thickness of the layers, as well as the probing frequency. Here, we model electromagnetic behaviour of stratified CO_2 ice and dust-laden H_2O ice, by assuming a 1D geometry (Lombardo et al., 2000; Pettinelli et al., 2003; Kartashov et al., 2004; Nunes and Phillips, 2006; Courville et al., 2021). Specifically, we simulate the propagation of radar pulses through twelve idealized models of the SPLD, consisting of sets of perfectly parallel planar interstratified basal layers composed of CO_2 ice and H_2O ice, where the latter has variable contents of dust. The total thickness of the simulated deposits was set at the value derived through MARSIS radargrams over the study area (1.5 km). The material underlying the deposits was set to be basaltic rock. The simulations were run by code adapted from MATLAB(TM) scripts publicly available through a public research data repository (Orosei and Cicchetti, 2018). The code computes the complex reflectivity of the layer stack across the range of frequencies within the pulse bandwidth, multiplying it by the signal spectrum and Inverse-Fourier transforming to the time domain. Simulations were run for one, two or three CO_2 ice layers, the lowermost of which is in direct contact with the bedrock, while the remaining ones are separated by layers of H_2O ice of variable thickness (Fig. 9). CO_2 ice layers are assumed to be lossless.

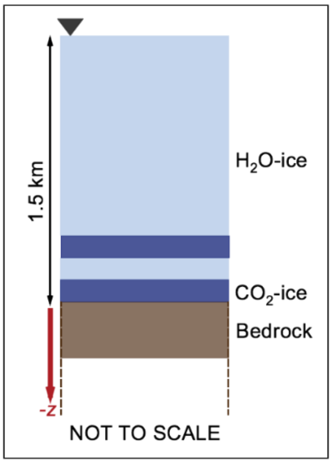

Fig. 9. Schematic stratigraphy used in numerical simulations. The model stratigraphy is here shown as a set of planar parallel layers of CO_2 ice (dark blue) and H_2O ice (light blue), bounded by an upper half space representing the Martian atmosphere (as semi-infinite vacuum) and a lower half space representing the Martian bedrock (brown). Simulations are run for one, two or three lossless CO_2 ice layers, the lowermost of which is in direct contact with the bedrock, while the remaining ones are separated by layers of H_2O ice of variable thickness. The topmost layer of H_2O ice represents the bulk of the stratigraphy. Layer thicknesses of CO_2 ice and interlayer dusty water ice range from 0 to up to 100 m, with total deposit thickness = 1.5 km. The red arrow indicates the depth direction (-*z*). The inverted triangle on top of the sequence indicates the surface of the deposits. The sketch is drawn not to scale.

Typically, complex relative dielectric permittivities are strongly dependent on the frequency of the propagating electromagnetic wave and the temperature of the medium. Attenuation of the signal is independent of frequency at MARSIS wavelength for pure water ice: we used the empirical formulae reported by Mätzler (1998) for the average surface temperature value of 160 K (Clifford, 1987) taken as a constant across the entire model stratigraphy. We find that the real part of the dielectric permittivity of water ice is 3.11, with loss tangent values between $2.5{\cdot}10^{-8}$ (3 MHz) and $3.7{\cdot}10^{-8}$ (5 MHz). The loss tangent of CO_2 ice is not well constrained at the temperature of interest, with extrapolations and upper limits only being reported in the published literature. In our computations therefore, we set it to be = 0, to produce the highest possible subsurface-to-surface echo power ratio values. We did not consider the effect of the complex part of the permittivity of CO_2 on the reflection coefficient, because it is generally assumed to be low ($\leq 10^{-3}$). Computing the Fresnel reflection coefficient at normal incidence for an interface between a layer of CO_2 ice and an underlying bedrock with permittivity values such as those used in the simulations, the results, with and without the inclusion of the imaginary part, differ by < 0.00001.

3.6. Simulations

To calculate the simulated radar waveforms, in our model stratigraphies we assumed perfectly smooth surfaces, an assumption that holds also for small roughness of the illuminated surface, where “small roughness” is defined (Ulaby et al., 1981) by a height < λ /32, which gives a value of 2.35 m at 4MHz. We considered the electromagnetic wave transmitted by the radar having a normal incidence with respect to the model stratified structure (ref. to sketch in Fig. 9), and assumed a 1D-model where the only variation of the electromagnetic properties occurs along the *z*-axis (depth). Furthermore, we assumed spatially homogenous layers with a constant complex dielectric permittivity (ε_i) and thickness (h_i). The stratified structure is bounded by two half-spaces representative of the atmosphere and the bedrock. This model is the same adopted in previous work (Orosei et al., 2018a; Lauro et al., 2019, Lalich et al., 2021a, 2021b). The received signal $y(t)$ is thus computed as:

$$y(t) = \mathcal{F}^{-1}[X(f)R(f)], \quad (1)$$

where $\mathcal{F}^{-1}$is the inverse Fourier transform, $X(f)$ is the Fourier transform of the signal transmitted by MARSIS antenna, $R(f)$ is the frequency response ($\Gamma_1(f)$) of the layered structure computed from the recursive scattering function $\Gamma_i(f)$:

$$R(f) = \Gamma_1(f)$$
$$\Gamma_i(f) = \frac{\rho_i + \Gamma_{i+1} e^{-2jk_{i+1}h_{i+1}}}{1+\rho_i \Gamma_{i+1} e^{-2jk_{i+1}h_{i+1}}}, \quad (3)$$

with k_i the complex-valued wavenumber of the *i*-th layer, and ρ_i the Fresnel reflection coefficient at the boundary between layer *i*–1 and *i*, given by:

$$\rho_i = \frac{\sqrt{\varepsilon_{i-1}} - \sqrt{\varepsilon_i}}{\sqrt{\varepsilon_{i-1}} + \sqrt{\varepsilon_i}}, \quad (4)$$

The geometry of the problem is modelled as a layered structure, where the upper and lower half space are the same for each simulation, whereas the assumed stratified layer between the atmosphere and the bedrock changes on the basis of the number of CO_2 ice layers, and the thickness of the layers. The ratio between basal and surface power is determined by considering the ratio between the maximum of the square amplitude of $y(t)$ at a time interval containing the echo return from the surface, and that occurring at a time interval containing the echo return from the upper side of the shallower CO_2 ice layer.

Using a multiprocessor machine, we simulated the three CO_2 layer model for every layer thickness between 0 and 50 m at 1-m intervals for three CO_2 layers and two intervening H_2O layers, for a total of 51^5 simulations. This allowed us to sample completely the parameter space of the models with two- and three-basal CO_2 layers, and thus to locate and explore the properties of local maxima embedded in the three- and five-parameter spaces respectively. We identified local maxima of subsurface to surface power ratio, both at 4 and 5 MHz, and for each of them we extracted the basal echo power ratio for all simulations whose layers are within 2 m of the thickness of those corresponding to the local maximum, thus simulating the effect of random but limited variation of the stratigraphy.

4. Results

To implement a quantitative comparison between data and simulation results, for each local maximum of subsurface to surface echo power ratio we produced the histogram of power values extracted from its neighbourhood, and convolved it with the template distributions shown in Figure 8, obtaining a simulated histogram which represents the global effect of the factors affecting propagation within the SPLD on model results. An example of a synthetic distribution is shown in Figure 10.

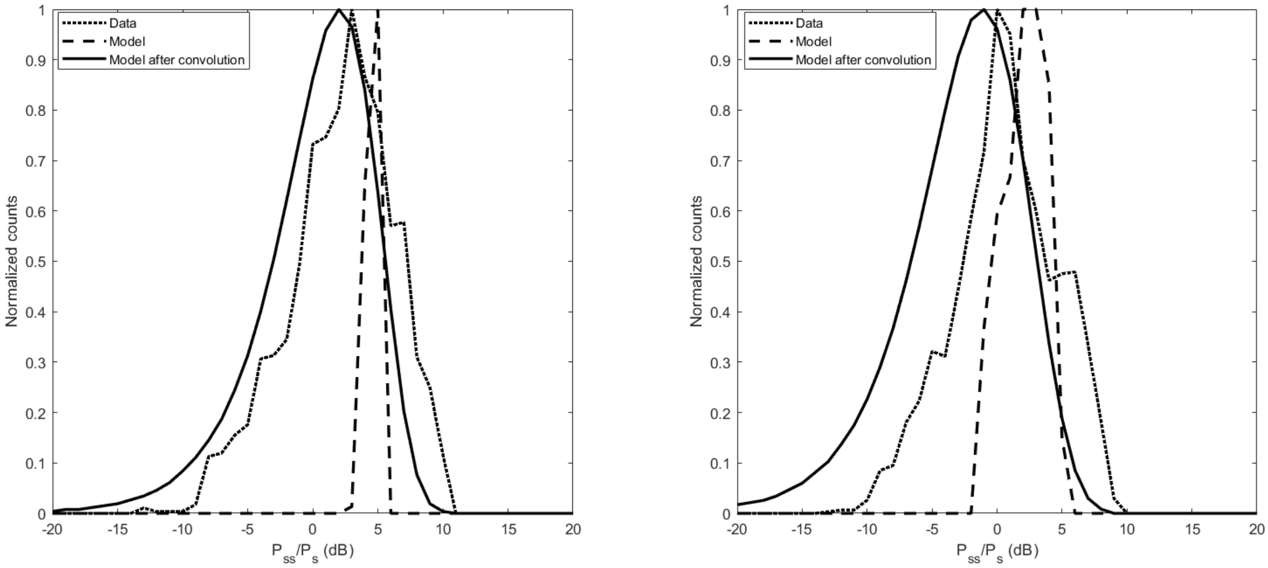

Fig. 10. Comparison between the histogram of measured values of subsurface to surface echo power ratio at 4 (left) and 5 MHz (right) with the histogram of model results in the neighbourhood of a given local maximum (see text for details), and with the synthetic histogram of model results produced through the convolution of the histogram of model results with the distribution template shown in Figure 8. The histograms are computed both for model results at 4 and 5 MHz.

To make a quantitative comparison of model results with data, the synthetic histograms were used to generate a set of random values representing measurements. This was done by taking each histogram bin, and generating a set of uniformly distributed random numbers in an interval corresponding to the bin, whose quantity is proportional to the bin height. Finally, the set of synthetic measurements was compared to actual measurements through a statistical test to determine if the two sets of samples could be produced by the same distribution. We used the two-sample Kolmogorov-Smirnov test (Kolmogorov, 1933; Smirnov, 1939), which is a nonparametric test for the null hypothesis that the data in two sets of samples are from the same continuous distribution. It is widely employed in statistics for its robustness and its sensitivity to both location and shape of distributions. The test was performed using the implementation available in the MATLAB(TM) proprietary programming language, and setting the significance level for the rejection of the null hypothesis at 5%.

A configuration of layers producing a local maximum at one frequency does not result in a local maximum at the other frequency. For this reason, both local maxima at 4 MHz and at 5 MHz had to be considered. Thus, for a given model (either two- or three-CO_2 ice layers) we simultaneously tested samples of model results at 4 and 5 MHz extracted for a set of layer thicknesses corresponding to a local peak of basal echo power at either 4 or 5 MHz, and for all layer thicknesses within two meters of the one producing the peak. This resulted in four possible combinations of number of layers and frequency of the echo power maximum. We found and tested 487 local maxima at 4 MHz and 687 at 5 MHz for the two-layer model, and 2981 local maxima at 4 MHz and 5232 at 5 MHz for the three-layer model. Results are shown in Figure 11.

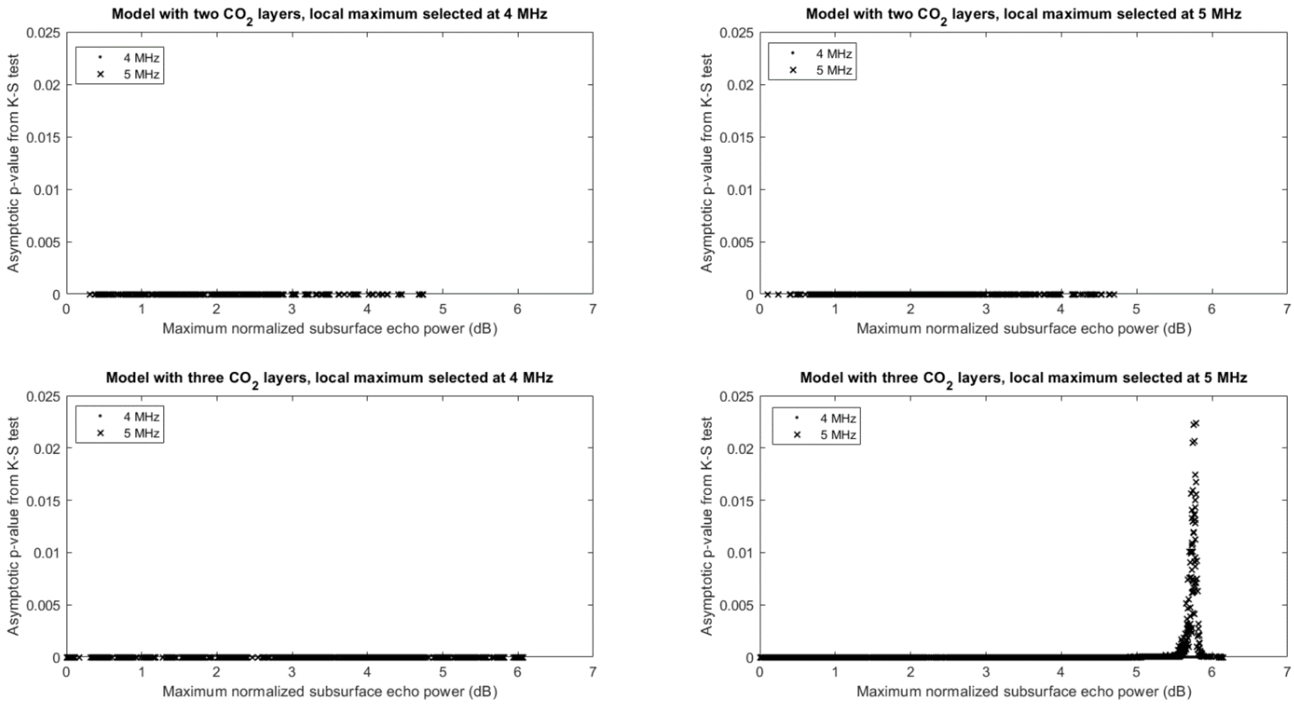

Fig. 11. Plots of the asymptotic p-values produced by the Kolmogorov-Smirnov test versus the maximum subsurface to surface power ratio of simulated echoes, for models with two- and three-CO_2 ice layers and for local maxima at 4 and 5 MHz. Each point represents the probability that model results and MARSIS measurements belong to the same continuous distribution. For each tested set of simulations, probabilities are computed both at 4 MHz (dots) and at 5 MHz (crosses).

No set of two- and three-layer models resulted in simulated values exceeding the 5% significance level threshold. However, it can be seen in the bottom right plot in Figure 11 that a few layer configurations resulting in a local maximum of basal echo power at 5 MHz approach the 5% threshold. This happens only at 5 MHz (crosses in Fig. 11), while at 4 MHz (dots) the probability remains negligible. This quantitatively confirms the observation that, in a model based on the coherent interference between layers, a configuration capable of producing a constructive interference at one frequency is not capable of doing the same at another frequency.

None of the modelled scenarios involving CO_2 ice layers reproduce the distribution of basal echo intensities observed by MARSIS over the bright areas in Ultimi Scopuli. Median values of the simulated basal echo power are lower than those observed in real MARSIS data, and the spread of the simulated values does not match the range of the measured data. We thus conclude that the interpretation that best reconciles all radar observations in Ultimi Scopuli remains that of a strong basal reflector overlain by a thick dust-laden SPLD.

5. Conclusions

The results of our simulations do not support claims that CO_2 ice layers interbedded with water ice can produce the bright reflections detected by MARSIS from the base of the SPLD in Ultimi Scopuli. Therefore, we rule out the presence of hidden deposits of basal CO_2 ice in this area. Based on these results, and the lack of detection of sequestered CO_2 ice deposits elsewhere in the SPLD (Whitten et al., 2017; Whitten and Campbell, 2018; Khuller and Plaut, 2021) beyond those reported by Phillips et al. (2011) and Bierson et al. (2016), we posit that it is unlikely that hidden CO_2 was stored in the late Amazonian (< 250 Ma) south polar deposits. This conclusion is consistent with the geological record of diminishing volcanic activity on Mars during the Hesperian and throughout the Amazonian, with very small amounts of CO_2 released into the atmosphere by volcanic degassing in post-Noachian times.

With the polar caps being the most voluminous reservoir of volatiles on Mars, and their role in regulating the planetary climate, records of the composition and physical properties of the polar layered deposits are fundamental to constrain the entire geological and climatological history of Mars. The ground penetrating radar MARSIS continuing acquisition of observations over the polar regions is an essential element of our investigations into the origin, evolution, and inventory of Martian volatiles and of the planet evolution. This is why interpretations of MARSIS data must be critically assessed against the framework of the physical theory of the propagation of radar waves through stratified media, as we have demonstrated in this paper. Rigorous application of this approach to all investigations based on MARSIS data will advance our knowledge of the nature and properties of Mars's polar materials.

Acknowledgments

The authors are grateful to A.P. Rossi and L. Guallini for their helpful comments on an earlier version of this manuscript. We thank two anonymous reviewers for their constructive criticism and insights, that contributed to clarify and improve the paper. This work was supported by the Italian Space Agency (ASI) through contract ASI-INAF 2019–21-HH.0.

References

Baker, V.R., 2001. Water and the martian landscape. Nature 412, 228-236 https://doi.org/10.1038/35084172.

Baker, V.R., Strom, R., Gulick, V., Kargel, J.S., Komatsu, G., Kale, V.S., 1991. Ancient oceans, ice sheets and the hydrological cycle on Mars. Nature 352, 589-5994 https://doi.org/10.1038/352589a0.

Becerra, P., Sori, M.M., Thomas, N., Pommerol, A., Simioni, E., Sutton, S.S., Tulyakov, S., Cremonese, G., 2019. Timescales of the climate record in the south polar ice cap of Mars. Geophys. Res. Lett. 46 (13), 7268-7277 https://doi.org/10.1029/2019GL083588.

Bierson, C.J., Phillips, R.J., Smith, I.B., Wood, S.E., Putzig, N.E., Nunes, D., Byrne, S., 2016. Stratigraphy and evolution of the buried CO_2 deposit in the Martian south polar cap. Geophys. Res. Lett. 43, 4172-4179 https://doi.org/10.1002/2016GL068457.

Bierson, C.J., Tulaczyk, S., Courville, S.W., Putzig, N.E., 2021. Strong MARSIS radar reflections from the base of Martian south polar cap may be due to conductive ice or minerals. Geophys. Res. Lett. 48(13), e2021GL093880 https://doi.org/10.1029/2021GL093880.

Bridges, J.C., Hicks, L.J., Treiman, A.H., 2019. Carbonates on Mars. In: Filiberto, J. & Schwenzer, S.P. (Eds.) Volatiles in the Martian Crust, pp 89-118 http://dx.doi.org/10.1016/B978-0-12-804191-8.00005-2.

Broquet, A., Wieczorek, M.A., Fa, W., 2021. The composition of the south polar cap of Mars derived from orbital data. J. Geophys. Res. Planets 126(8), e2020JE006730 https://doi.org/10.1029/2020JE006730.

Brown, A.J., Piqueux, S., Titus, T.N., 2014. Interannual observations and quantification of summertime H_2O ice deposition on the Martian CO_2 ice south polar cap. Earth Planet. Sci. Lett. 406, 102-109 http://dx.doi.org/10.1016/j.epsl.2014.08.039.

Buhler, P.B., Ingersoll, A.P., Piqueaux, S., Ehlmann, B.L., Hayne, P.O., 2021. Coevolution of Mars's atmosphere and massive south polar CO_2 ice deposit. Nature Astronomy 4, 363-371 https://doi.org/10.1038/s41550-019-0976-8.

Byrne, S., Ingersoll, A.P., 2003. A sublimation model for Martian south polar ice features. Science 299, 1051-1053 http://science.sciencemag.org/content/299/5609/1051.

Catling, D.C., 2014. Mars atmosphere: History and surface interactions. In: Spohn et al. (Eds.) Encyclopedia of the Solar System, ch. 16, pp. 343- 357 http://dx.doi.org/10.1016/B978-0-12-415845-0.00016-5.

Clifford, S.M., 1987. Polar basal melting on Mars. J. Geophys. Res. 92 (B9), 9135-9152 https://doi.org/10.1029/JB092iB09p09135.

Courville, S.W., Perry, M.R., Putzig, N.E., 2021. Lower bounds on the thickness and dust content of layers within the North Polar Layered Deposits of Mars from radar forward modelling. Planet. Sci. J. 2, 28 https://doi.org/10.3847/PSJ/abda50.

Edwards, C.S., Ehlmann B.L., 2015. Carbon sequestration on Mars. Geology 43(1), 863-866 https://doi.org/10.1130/G36983.1.

Forget, F., Wordsworth, R., Millour, E., Madeleine, J.-B., Kerber, L., Leconte, J., Marcq, E., Haberle, R.M., 2013. 3D modelling of the early martian climate under a denser CO_2 atmosphere: Temperatures and CO_2 ice clouds. Icarus 222, 81-99 http://dx.doi.org/10.1016/j.icarus.2012.10.019.

Grima, C., Kofman, W., Herique, A., Orosei, R., Seu, R. 2012. Quantitative analysis of Mars surface radar reflectivity at 20 MHz. Icarus 220, 84–99. doi:10.1016/j.icarus.2012.04.017

Grott, M., Baratoux, D., Hauber, E., Sautter, V., Mustard, J., Gasnault, O., Ruff, S.W., Karato, S.-I., Debaille, V., Knapmeyer, M., Sohl, F., Van Hoolst, T., Breuer, D., Morschhauser, A., Toplis, M.J., 2013. Long-term evolution of the Martian crust-mantle system. Space Sci. Rev. 174, 49-111 https://doi.org/10.1007/s11214-012-9948-3.

Grott, M., Morschhauser, A., Breuer, D., Hauber, E., 2011. Volcanic outgassing of CO_2 and H_2O on Mars. Earth Planet. Sci. Lett. 308 (3-4), 391-400 https://doi.org/10.1016/j.epsl.2011.06.014.

Guallini, L., Rossi, A.P., Forget, F., Marinangeli, L., Lauro, S.E., Pettinelli, E., Seu, R., Thomas, N., 2018. Regional stratigraphy of the south polar layered deposits (Promethei Lingula, Mars): “Discontinuity-bounded” units in images and radargrams. Icarus 308, 76-107 http://dx.doi.org/10.1016/j.icarus.2017.08.030.

Gulick, V.C., Baker, V.R., 1989. Fluvial valleys and martian palaeoclimates. Nature 341, 514-516 https://doi.org/10.1038/341514a0.

Haberle, R.M., Tyler, D., McKay, C.P., Davis, W.L., 1994. A model for the evolution of CO_2 on Mars. Icarus 109, 102-120 https://doi.org/10.1006/icar.1994.1079.

Haynes, M. S., Chapin, E., Schroeder, D. M. 2018. Geometric Power Fall-Off in Radar Sounding. IEEE Transactions on Geoscience and Remote Sensing 56, 6571–6585. doi:10.1109/TGRS.2018.2840511

Hecht, M., Fisher, D.A., Catling, D.C., Kounaves, S., 2018. RE: Radar evidence of subglacial liquid water on Mars (Orosei et al.). Science eLetters 15 August 2018 https://science.sciencemag.org/content/361/6401/490/tab-e-letters.

Hecht, M.H., Kounaves, S.P., Quinn, R.C., West, S.J., Young, S.M.M., Ming, D., Catling, D.C., Clark, B.C., Boynton, W.V., Hoffman, J., DeFlores, L.P., Gospodinova, K., Kapit, J., Smith, P.H., 2009. Detection of perchlorate and the soluble chemistry of martian soil at the Phoenix lander site. Science 325 (5936), 64-67 https://doi.org/10.1126/science.1172466.

Herkenhoff, K.E., Plaut, J.J., 2000. Surface ages and resurfacing rates of the polar layered deposits on Mars. Icarus 144, 243-253 https://doi.org/10.1006/icar.1999.6287.

Hvidberg, C.S., Fishbaugh, K.E., Winstrup, M., Svensson, A., Byrne, S., Herkenhoff, K.E., 2012. Reading the climate record of the martian polar layered deposits. Icarus 221 (1), 405-419 https://doi.org/10.1016/j.icarus.2012.08.009.

Jakosky, B.M., 2019. The CO_2 inventory on Mars. Planet. Space Sci. 175, 52-59 https://doi.org/10.1016/j.pss.2019.06.002.

Jakosky, B.M., 2021. Atmospheric loss to space and the history of water on Mars. Annu. Rev. Earth Planet. Sci. 49, 71-93 https://doi.org/10.1146/annurev-earth-062420-052845.

Jakosky, B.M., Henderson, B.G., Mellon, M.T., 1995. Chaotic obliquity and the nature of the Martian climate. J. Geophys. Res. Planets 100, 1579-1584 https://doi.org/10.1029/94JE02801.

Jonard, F., André, F., Pinel, N., Warren, C., Vereecken, H., Lambot, S. 2019. Modeling of Multilayered Media Green’s Functions With Rough Interfaces. IEEE Transactions on Geoscience and Remote Sensing 57, 7671-7681. doi: 10.1109/TGRS.2019.2915676.

Jones, E., Caprarelli, G., Mills, F.P., Doran, B., Clarke, J., 2014. An alternative approach to mapping thermophysical units from Martian thermal inertia and albedo data using a combination of unsupervised classification techniques. Remote Sensing 6, 5184-5237 https://doi.org/10.3390/rs6065184.

Kartashov, D.V., Shchuko, O.B., Orosei, R., 2004. Radar detection of subsurface features on Mars. Advances in Space Research 33 (12), 2263-2269 https://doi.org/10.1016/S0273-1177(03)00525-8.

Kahn, R., 1985. The evolution of CO_2 on Mars. Icarus 62, 175-190 https://doi.org/10.1016/0019-1035(85)90116-2.

Khuller, A.R., Plaut, J.J., 2021. Characteristics of the basal interface of the Martian South Polar Layered Deposits. Geophys. Res. Lett. 38, e2021GL093631 https://doi.org/10.1029/2021GL093631.

Kolmogorov, A. N. 1933. Sulla determinazione empirica di una legge di distribuzione. Giornale dell’Istituto Italiano degli Attuari 4, 83–91.

Koutnik, M., Byrne, S., Murray, B., 2002. South Polar Layered Deposits of Mars: The cratering record. J. Geophys. Res. Planets 107 (E11), 5100, doi: 10.1029/2001JE001805 https://doi.org/10.1029/2001JE001805.

Lalich, D.E., Hayes, A.G., Poggiali, V., 2021a. Explaining bright radar reflections in the Martian SPLD without liquid water. Lunar Planet. Sci. Conf. LII, 2392.

Lalich, D. E., Hayes, A. G., Poggiali, V. 2021b. Explaining Bright Radar Reflections Below The Martian South Polar Layered Deposits Without Liquid Water. arXiv e-prints https://doi.org/10.48550/arXiv.2107.03497

Lauro, S.E., Pettinelli, E., Caprarelli, G., Guallini, L., Rossi, A.P., Mattei, E., Cosciotti, B., Cicchetti, A., Soldovieri, F., Cartacci, M., Di Paolo, F., Noschese, R., Orosei, R., 2021. Multiple subglacial water bodies below the south pole of Mars unveiled by new MARSIS data. Nature Astronomy 5, 63-70 https://doi.org/10.1038/s41550-020-1200-6.

Lauro, S.E., Soldovieri, F., Orosei, R., Cicchetti, A., Cartacci, M., Mattei, E., Cosciotti, B., Di Paolo, F., Noschese, R., Pettinelli, E., 2019. Liquid water detection under the South Polar Layered Deposits of Mars – A probabilistic inversion approach. Remote Sensing 11 (20), 2445 https://doi.org/10.3390/rs11202445.

Li, J., Andrew-Hanna, J.C., Sun, Y., Phillips, R.J., Plaut, J.J., Zuber, M.T., 2012. Density variations within the south polar deposits of Mars. J. Geophys. Res. Planets 117(E4), doi: 10.1029/2011JE003937 https://doi.org/10.1029/2011JE003937.

Lombardo, P., Magenta, A.M., Pettinelli, E., 2000. Multichannel fusion of subsurface radar images at different resolutions. IEE Proc. Radar, Sonar and Navigation 147 (3), 121-133 https://digital-library-theiet.org/content/journals/10.1049/ip-rsn_20000196.

Malin, M.C., Caplinger, M.A., Davis, S.D., 2001. Observational evidence for an active surface reservoir of solid carbon dioxide on Mars. Science 294 (5549), 2146-2148 https://science.sciencemag.org/content/294/5549/2146.

Manning, C.V., Bierson, C., Putzig, N.E., McKay, C.P., 2019. The formation and stability of buried polar CO_2 deposits on Mars. Icarus 317, 509-517 https://doi.org/10.1016/j.icarus.2018.07.021.

Mattei, E., Lauro, S.E., Vannaroni, G., Cosciotti, B., Bella, F., Pettinelli, E., 2014. Dielectric measurements and radar attenuation estimation of ice/basalt sand mixtures as martian Polar Caps analogues. Icarus 229, 428-433 https://doi.org/10.1016/j.icarus.2013.10.017.

Mätzler, C., 1998. Microwave properties of ice and snow. In: Schmitt B, De Bergh C, Festou M (Eds.) Solar System Ices. Astrophys. Space Sci. Library 227, 241-257 https://doi.org/10.1007/978-94-011-5252-5_10.

Mellon, M.T., 1996. Limits on the CO_2 content of the Martian polar deposits. Icarus 124, 268-279 https://doi.org/10.1006/icar.1996.0203.

Mellon, M.T., Feldman, W.C., Prettyman, T.H., 2004. The presence and stability of ground ice in the southern hemisphere of Mars. Icarus 169, 324-340 https://doi.org/10.1016/j.icarus.2003.10.022.

Michalski, J.R., Niles, P.B., 2010. Deep crustal carbonate rocks exposed by meteor impact in Mars. Nature Geoscience 3, 751-755 https://doi.org/10.1038/ngeo971.

Milkovich, S.M., Plaut, J.J., 2008. Martian South Polar Layered Deposit stratigraphy and implications for accumulation history. J. Geophys. Res. Planets 113, E06007, doi: 10.1029/2007JE002987 https://doi.org/10.1029/2007JE002987.

Milkovich, S.M., Plaut, J.J., Safaenili, A., Picardi, G., Seu, R., Phillips, R.J., 2009. Stratigraphy of the Promethei Lingula, south polar layered deposits, Mars, in radar and imaging datasets. J. Geophys. Res. Planets 114, E03002, doi: 10.1029/2008JE003162 https://doi.org/10.1029/2008JE003162.

Nunes, D.C., Phillips, R.J., 2006. Radar surface mapping of the polar layered deposits on Mars. J. Geophys. Res. Planets. 111 (E6), E06S21, doi: 10.1029/2005JE002609 https://doi.org/10.1029/2005JE002609.

Orosei, R., Cicchetti, A., 2018. Data files and electromagnetic simulation software used in the paper "Radar evidence of subglacial liquid water on Mars" by Orosei et al. (2018) [Data set]. Zenodo https://zenodo.org/record/1285179.

Orosei, R., Jordan, R.L., Morgan, D.D., Cartacci, M., Cicchetti, A., Duru, F., Gurnett, D.A., Heggy, E., Kirchner, D.L., Noschese, R., Kofman, W., Masdea, A., Plaut, J.J., Seu, R., Watters, T.R., Picardi, G., 2015. Mars Advanced Radar for Subsurface and Ionospheric Sounding (MARSIS) after nine years of operation: A summary. Planet. Space. Sci. 112, 98-114 https://doi.org/10.1016/j.pss.2014.07.010.

Orosei, R., Lauro, S.E., Pettinelli, E., Cicchetti, A., Coradini, M., Cosciotti, B., Di Paolo, F., Flamini, E., Mattei, E., Pajola, M., Soldovieri, F., Cartacci, M., Cassenti, F., Frigeri, A., Giuppi, S., Martufi, R., Masdea, A., Mitri, G., Nenna, C., Noschese, R., Restano, M., Seu, R., 2018a. Radar evidence of subglacial liquid water on Mars. Science 361 (6401), 490-493 http://science.sciencemag.org/content/361/6401/490.

Orosei, R., Lauro, S.E., Pettinelli, E., Cicchetti, A., Coradini, M., Cosciotti, B., Di Paolo, F., Flamini, E., Mattei, E., Pajola, M., Soldovieri, F., 2018b. RE: Response to Orosei et al., Radar evidence of subglacial liquid water on Mars, by Hecht, Fisher, Catling and Kounaves. Science eLetters 29 August 2018 https://science.sciencemag.org/content/361/6401/490/tab-e-letters.

Orosei, R. and 11 colleagues 2020. The Global Search for Liquid Water on Mars from Orbit: Current and Future Perspectives. Life 10, 120. doi:10.3390/life10080120.

Pestova, O.N., Myun, L.A., Khripun, M.K., Prigaro, A.V., 2005. Polythermal study of the systems $M(ClO_4)_2$-H_2O ($M^{2+} = Mg^{2+}$, Ca^{2+}, Sr^{2+}, Ba^{2+}). Russian J. of Appl. Chemistry 78 (13), 409-413 https://doi.org/10.1007/s11167-005-0306-z.

Pettinelli, E., Cosciotti, B., Di Paolo, F., Lauro, S.E., Mattei, E., Orosei, R., Vannaroni, G., 2015. Dielectric properties of Jovian satellite ice analogs for subsurface radar exploration: A review. Rev. Geophys. 53 (3), 593-641 https://doi.org/10.1002/2014RG000463.

Pettinelli, E., Vannaroni, G., Cereti, A., Paolucci, F., Della Monica, G., Storini, M., Bella, F., 2003. Frequency and time domain permittivity measurements on solid CO_2 and solid CO_2-soil mixtures as Martian soil simulants. J. Geophys. Res. Planets 108 (E4), 8029, doi: 10.1029/2002JE001869 https://doi.org/10.1029/2002JE001869.

Phillips, R.J., Davis, B.J., Tanaka, K.L., Byrne, S., Mellon, M.T., Putzig, N.E., Haberle, R.M., Kahre, M.A., Campbell, B.A., Carter, L.M., Smith, I.B., Holt, J.W., Smrekar, S.E., Nunes, D.C., Plaut, J.J., Egan, A.F., Titus, T.N., Seu, R., 2011. Massive CO_2 ice deposits sequestered in the South Polar Layered Deposits of Mars. Science 332 (6031), 838-841 https://science.sciencemag.org/content/332/6031/838.

Picardi, G., Biccari, D., Seu, R., Marinangeli, L., Johnson, W.T.K., Jordan, R.L., Plaut, J., Safaenili, A., Gurnett, D.A., Ori, G.G., Orosei, R., Calabrese, D., Zampolini, E., 2004. Performance and surface scattering models for the Mars Advanced Radar for Subsurface and Ionosphere Sounding (MARSIS). *Planet. Space. Sci.* **52**, 149-156 https://doi.org/10.1016/j.pss.2003.08.020.

Plaut, J.J., Picardi, G., Cicchetti, A., Clifford, S., Edenhofer, P., Farrell, W., Federico, C., Frigeri, A., Heggy, E., Herique, A., Ivanov, A., Jordan, R., Kofman, W., Leuschen, C., Marinangeli, L., Nielsen, E., Ori, G., Orosei, R., Pettinelli, E., Phillips, R., Plettemeier, D., Safaenili, A., Seu, R., Stofan, E., Vannaroni, G., Watters, T., Williams, I., 2006. MARSIS subsurface sounding observations of the South Polar Layered Deposits. Lunar Planet. Sci. Conf. XXXVII, 1211.

Plaut, J.J., Picardi, G., Safaenili, A., Ivanov, A.B., Milkovich, S.M., Cicchetti, A., Kofman, W., Mouginot, J., Farrell, W.M., Phillips, R.J., Clifford, S.M., Frigeri, A., Orosei, R., Federico, C., Williams, I.P., Gurnett, D.A., Nielsen, E., Hagfors, T., Heggy, E., Stofan, E.R., Plettemeier, D., Watters, T.R., Leuschen, C.J., Edenhofer, P., 2007. Subsurface radar sounding of the South Polar Layered Deposits of Mars. Science 316 (5281), 92-95 http://science.sciencemag.org/content/316/5821/92.

Plesa, A.-C., Padovan, S., Tosi, N., Breuer, D., Grott, M., Wieczorek, M.A., Spohn, T., Smrekar, S.E., Banerdt, W.B., 2018. The thermal state and interior structure of Mars. Geophys. Res. Lett. 45, 12198-12209 https://doi.org/10.1029/2018GL080728.

Primm, K.M., Gough, R.V., Chevrier, V.F., Tolbert, M.A., 2017. Freezing of perchlorate and chloride brines under Mars-relevant conditions. Geochim. Cosmochim. Acta 212, 211-220 https://doi.org/10.1016/j.gca.2017.06.012.

Porcello, L. J. and 7 colleagues 1974. The Apollo lunar sounder radar system. IEEE Proceedings 62, 769–783.

Putzig, N.E., Mellon, M.T., Kretke, K.A., Arvidson, R.E., 2005. Global thermal inertia and surface properties of Mars from the MSG mapping mission. Icarus 173 (2), 325-341 https://doi.org/10.1016/j.icarus.2004.08.017.

Putzig, N.E., Smith, I.B., Perry, M.R., Foss, F.J., Campbell, B.A., Phillips, R.J., Seu, R., 2018. Three-dimensional radar imaging of structures and craters in the Martian polar caps. Icarus 308, 138-147 https://doi.org/10.1016/j.icarus.2017.09.023.

Ramirez, R.M., Craddock, R.A., 2018. The geological and climatological case for a warmer and wetter early Mars. Nature Geoscience 11, 230-237 https://doi.org/10.1038/s41561-018-0093-9.

Sasaki, Y., Shang, F., Kidera, S., Kirioto, T., Saho, K., Sato, T., 2017. Three-dimensional imaging method incorporating range points migration and Doppler velocity estimation for UWB millimeter-wave radar. IEEE Geosci. Remote Sens. Lett. 14 (1), 122-126, doi: 10.1109/LGRS.2016.2628909 https://doi.org/10.1109/LGRS.2016.2628909.

Schroeder, D.M., Steinbrügge, G., 2021. Alternatives to liquid water beneath the south polar ice cap of Mars. Geophys. Res. Lett. 48(19), e2021GL095912 https://doi.org/10.1029/2021GL095912.

Sihvola, A., 2000. Mixing rules with complex dielectric coefficients. Subsurface Sensing Technologies and Applications 1, 393-415 https://doi.org/10.1023/A:1026511515005.

Simpson, R.A., Fair, B.C., Howard, H.T., 1980. Microwave properties of solid CO_2. J. Geophys. Res. 85 (B10), 5481-5484 https://doi.org/10.1029/JB085iB10p05481.

Smirnov, N. V. 1939. Estimate of deviation between empirical distribution functions in two independent samples. (Russian). Bull. Moscow Univ. 2, 3–16.

Smith, I.B., Hayne, P.O., Byrne, S., Becerra, P., Kahre, M., Calvin, W., Hvidberg, C., Milkovich, S., Buhler, P., Landis, M., Horgan, B., Kleinböhl, A., Perry, M.R., Obbard, R., Stern, J., Piqueaux, S., Thomas, N., Zacny, K., Carter, L., Edgar, L., Emmett, J., Navarro, T., Hanley, J., Koutnik, M., Putzig, N., Henderson, B.L., Holt, J.W., Ehlmann, B., Parra, S., Lalich, D., Hansen, C., Hecht, M., Banfield, D., Herkenhoff, K., Paige, D.A., Skidmore, M., Staehle, R.L., Siegler, M., 2020. The Holy Grail: A road map for unlocking the climate record stored within Mars' polar layered deposits. Planet. Space Sci. 184, 104841 https://doi.org/10.1016/j.pss.2020.104841.

Smith, I.B., Lalich, D.E., Rezza, C., Horgan, B.H.N., Whitten, J.L., Nerozzi, S., Holt, J.W., 2021. A solid interpretation of bright radar reflectors under the Mars south polar ice. Geophys. Res. Lett. 48(15), e2021GL093618 https://doi.org/10.1029/2021GL093618.

Sori, M.M., Bramson, A.M., 2019. Water on Mars, with a grain of salt: Local heat anomalies are required for basal melting of ice at the south pole today. *Geophys. Res. Lett.* **46**, 1222-1231 https://doi.org/10.1029/2018GL080985.

Tanaka, K.L., Kolb, E.J., 2001. Geological history of the polar regions of Mars based on Mars Global Surveyor data: I. Noachian and Hesperian periods. Icarus 154, 3-21 https://doi.org/10.1006/icar.2001.6675.

Tanaka, K.L., Skinner, J.A., Dohm, J.M., Irwin, R.P., Kolb, E.J., Fortezzo, C.M., Platz, T., Michael, G.G., Hare, T.M., 2014. Geologic map of Mars. USGS Sci. Invest. Map 3292, scale 1:20,000,000.

Thomas, P.C., Calvin, W.M., Gierasch, P., Haberle, R., James, P.B., Sholes, S., 2013. Time scales of erosion and deposition recorded in the residual south polar cap of Mars. Icarus 225 (2), 923-932 https://doi.org/10.1016/j.icarus.2012.08.038.

Toner, J.D., Catling, D.C., Light, B., 2014. The formation of supercooled brines, viscous liquids, and low-temperature perchlorate glasses in aqueous solutions relevant to Mars. *Icarus* **233**, 36-47 https://doi.org/10.1016/j.icarus.2014.01.018.

Ulaby, F.T., Moore, R.K., Fung, A.K., 1981. Microwave Remote Sensing – Active and Passive, vol. II. Artech House, Norwood, 921-949.

Whitten, J.L., Campbell, B.A., 2018. Lateral continuity of layering in the Mars South Polar Layered Deposits from SHARAD sounding data. J. Geophys. Res. Planets 123, 1541-1554 https://doi.org/10.1029/2018JE005578.

Whitten, J.L., Campbell, B.A., Morgan, G.A., 2017. A subsurface depocenter in the South Polar Layered Deposits of Mars. Geophys. Res. Lett. 44, 8188-8195 https://doi.org/10.1002/2017GL074069.

Wray, J.J., Murchie, S.L., Bishop, J.L., Ehlmann, B.L., Milliken, R.E., Wilhelm, M.B., Seelos, K.D., Chojnacki, M., 2016. Orbital evidence for more widespread carbonate-bearing rocks on Mars. J. Geophys. Res. Planets 121, 652-677 https://doi.org/10.1002/2015JE004972.

Zuber, M.T., Phillips, R.J., Andrews-Hanna, J.C., Asmar, S.W., Konopliv, A.S., Lemoine, F.G., Plaut, J.J., Smith, D.E., Smrekar, S.E., 2007. Density of Mars' South Polar Layered Deposits. *Science* **317** (5845), 1718-1719 http://science.sciencemag.org/content/317/5845/1718.

Numerical simulations of radar echoes rule out basal CO_2 ice deposits at Ultimi Scopuli, Mars.

Roberto Orosei[1], Graziella Caprarelli[2]*, Sebastian Lauro[3], Elena Pettinelli[3], Marco Cartacci[4], Andrea Cicchetti[4], Barbara Cosciotti[3], Alessandro De Lorenzis[5], Giorgio De Nunzio[6,7], Elisabetta Mattei[3], Carlo Nenna[8], R. Noschese[4], Francesco Soldovieri[9].

[1]. Istituto Nazionale di Astrofisica, Istituto di Radioastronomia, Via Piero Gobetti 101, 40127 Bologna, Italy.
[2]. University of Southern Queensland, Centre for Astrophysics, West St, Darling Heights QLD 4350, Australia.
[3]. Università degli Studi Roma Tre, Dipartimento di Matematica e Fisica, Via della Vasca Navale 84, 00146 Rome, Italy.
[4]. Istituto Nazionale di Astrofisica, Istituto di Astrofisica e Planetologia Spaziali, Via del Fosso del Cavaliere, 100, 00133 Roma, Italy.
[5]. Centro euro-Mediterraneo sui Cambiamenti Climatici, Divisione Ocean Predictions and Applications, Via Marco Biagi 5, 73100 Lecce, Italy.
[6]. Università del Salento, Dipartimento di Matematica e Fisica "Ennio de Giorgi", Via Provinciale per Arnesano, 73100 Lecce, Italy.
[7]. Istituto Nazionale Fisica Nucleare, Sezione di Lecce, Via Provinciale per Arnesano, 73100 Lecce, Italy.
[8]. Enginium S.r.l., Via Luigi Cadorna 67, 20090 Vimodrone, Italy.
[9]. Consiglio Nazionale delle Ricerche, Istituto per il Rilevamento Elettromagnetico dell'Ambiente, Via Diocleziano 328, 80124 Naples, Italy.

* Corresponding author: Graziella.Caprarelli@usq.edu.au

Abstract

The principal objective of the radar sounder MARSIS experiment is to look for ice and water in the Martian subsurface. One particular focus of investigations, since 2005, has been the search for basal liquid water in the south polar layered deposits (SPLD). Anomalously strong basal echoes detected from four distinct areas at the base of the deposits at Ultimi Scopuli have been interpreted to indicate the presence of bodies of liquid water in this location, beneath a 1.5 km thick cover of ice and dust. Other explanations for the bright basal reflections have been proposed, however, including the possibility of constructive interference in layered media. Here, we test this mechanism through simulations of MARSIS radar signals propagating in models of CO_2-H_2O ice sequences. We then compare the results to real MARSIS data acquired over Ultimi Scopuli, finding that no CO_2-H_2O ice model sequence reproduces the set of real data. The results of our work have implications in relation to the global CO_2 inventory of Mars.

Keywords: Mars, SPLD, MARSIS, CO_2 ice, radar.

1. Introduction

The radar sounder MARSIS (Mars Advanced Radar for Subsurface and Ionospheric Sounding) on board the European Space Agency orbiter Mars Express, has been probing the Martian subsurface since 2005 (Orosei et al., 2015), exploring the global distribution of rock, soil, ice, and liquid water. The instrument operates within the range 1.3-5.5 MHz, transmitting a 1 MHz-bandwidth pulse centered at the frequencies of 1.8, 3, 4 and 5 MHz. Exploration of the Martian subsurface is mostly carried out using the 3 and 4 MHz, or 4 and 5 MHz frequencies, for a nominal depth of investigation of up to 5 km, depending on the electromagnetic properties of the probed material (Picardi et al., 2004).

The primary objective for the MARSIS experiment is to look for buried ice and water in the Martian subsurface. It was not until 2018, however, that evidence of bright subsurface reflections originating 1.5 km deep below the surface of Ultimi Scopuli, one of the terminal regions of the South Polar Layered Deposits (SPLD), was obtained (Orosei et al., 2018a) at coordinates 193°E - 81°S. The reflections, much brighter than those detected from the surface, were interpreted as originating from basal ponded water or wet sediments distributed on an area approximately 20 km across. The work reignited the scientific debate about the stability of liquid water at the Martian polar regions, and specifically at the south pole, where average surface temperatures (Mellon et al., 2004) are estimated to be 162 K. A possible explanation for the water being liquid at these conditions is that it contains a high concentration of salts (e.g., perchlorates, chlorides) which are ubiquitous on Mars (Hecht et al., 2009) and have eutectic temperatures as low as 198 K (Pestova et al., 2005). It was subsequently suggested that a high geothermal gradient, such as that produced by a magmatic chamber at depth, is required to reach the eutectic temperatures of concentrated salt solutions at the base of the deposits (Sori and Bramson, 2019). This scenario was disputed, however, on the grounds that there is no evidence of an anomalous geothermal gradient in the region (Lauro et al., 2021). Newly acquired MARSIS orbits of the region further revealed other three previously undetected areas of bright reflections, each approximately 10 km across (Lauro et al., 2021). Because laboratory experiments have shown that hypersaline aqueous solutions can form and persist over time at temperatures as low as 123 K, well below their eutectic temperatures (Toner et al., 2014; Primm et al., 2017), a hypersaline origin of the water was deemed to remain the most likely explanation for the bright reflections (Lauro et al., 2021). It is however difficult to envisage how large bodies of supercooled brines could have persisted in the natural Martian environment over geological timescales (Schroeder and Steinbrügge, 2021; Smith et al., 2021), which remains a significant argument against the liquid brine interpretation. The possibility that bright reflections could be caused by scattering phenomena in a stratified medium was also raised (Hecht et al., 2018). This criticism was however dismissed by Orosei et al. (2018b), who pointed out that they had demonstrated that the strength of the basal echoes at Ultimi Scopuli cannot be explained by multiple reflections. Even though a particular stratigraphic arrangement could produce enhanced basal echoes at one of the MARSIS frequencies of detection, it did not do so at the other observation frequencies. Alternative models suggesting that a range of materials, other than bodies of liquid water, could explain the sources of the strong basal echoes, have recently been published by Bierson et al. (2021), and Smith et al. (2021). The merits of all proposed alternative hypotheses have been reviewed by Schroeder and Steinbrügge (2021), who argued that none of the alternatives is conclusively incompatible with bodies of liquid water as the source of the bright basal reflections, and that each model opens up questions providing new opportunities for future investigations.

Distinct layers of CO_2 ice have been detected by radar sounder SHARAD surveys of the SPLD (Phillips et al., 2011; Bierson et al., 2016). The layers, up to 1 km thick, are interlayered with thin (typically 10-40 m thick) water ice, and it has been calculated that sublimation of these massive deposits of CO_2 ice would increase the Martian atmospheric pressure by 100% (Bierson et al., 2016). It has been suggested that, if the conditions leading to formation of the thick CO_2-H_2O ice deposits have occurred at other times, during the approximately 100 Myr history of formation of the SPLD (Manning et al., 2019), then a specific CO_2 ice layering configuration might produce subsurface reflections of higher intensity than those from the surface. In fact, Lalich et al. (2021a,b) obtained strong simulated radar reflections at 4 MHz frequency, mimicking MARSIS waveform, for a model configuration involving 1-100 m thick basal CO_2 ice layers sandwiching a dusty water ice layer of comparable thickness. Such configuration over the extent of MARSIS bright area, would translate in an average ~ 2% of the current CO_2 atmospheric content. While this specific contribution to the atmospheric volatile budget appears negligible, compounding scenarios involving storage of volatiles within the south polar cap can potentially impact estimates of the Martian volatile budget, with consequences on models of Martian climate cycles and atmospheric evolution, and on estimates of the amount of volatiles stored in the Martian crust as part of the geological record.

The Martian polar caps are the most voluminous exposed reservoirs of volatiles on Mars. It is estimated that, combined, the polar caps store two thirds of the entire water content of the planet (Catling, 2014; Smith et al., 2020; Jakoski, 2021). While climate models have suggested the possibility that the polar layered deposits may also contain significant amounts of CO_2 (Jakoski et al., 1995), estimates based on thermophysical properties of water and CO_2 ices rejected such interpretation (Mellon, 1996). The thin veneer of seasonal and residual solid CO_2 on the surface of the polar caps is effectively counted as part of the atmosphere (Jakosky, 2019). However, geomorphological (Gulick and Baker, 1989; Baker et al., 1991; Baker, 2001; Ramirez and Craddock, 2018) and geochemical evidence (Bridges et al., 2019) has been interpreted to indicate that early Mars was warmer and wetter than at present, prompting suggestions that a thick CO_2 rich atmosphere existed at the time, to account for greenhouse heating of the planet (Haberle et al., 1994). It has been argued that subsequent loss to space of the CO_2 (and other volatiles) does not fully account for the present-day content of CO_2 in the current thin Martian atmosphere, and that massive quantities of CO_2 ought to be sequestered within one or more geological sinks on Mars (Forget et al., 2013). While deep-seated carbonates could in principle accommodate large volumes of CO_2 (Kahn, 1985; Michalski and Niles, 2010; Wray et al., 2016; Jakosky, 2019), as is the case on Earth, there is at present no conclusive evidence for a global deep-crustal reservoir of carbonates on Mars (Edwards and Ehlmann, 2015). The discovery of massive deposits of CO_2 ice (Phillips et al., 2011; Bierson et al., 2016) in the South Polar Layered Deposits (SPLD) by the radar sounder SHARAD, and three-dimensional radar imaging volume calculations suggesting the deposits may contain more than $1.6 \cdot 10^4$ km^3 of dry ice (Putzig et al., 2018), have thus paved the way for renewed investigations into the possibility of the polar ice caps as CO_2 sinks.

The global abundance of CO_2 on Mars is presently unknown. There are some generally accepted points, however, that hold irrespective of the exact abundance and distribution of CO_2 on Mars. Mars had lost most of its CO_2 rich atmosphere by the end of the Noachian (~ 3.7 Ga) (Jakosky, 2019). The rate of input of juvenile gases into the atmosphere through planetary outgassing (i.e., volcanic activity) is not known precisely, but it was higher during the Noachian, waning in the Hesperian, becoming negligible in the Amazonian (Grott et al., 2011), so it would have been insufficient to replenish the lost early atmospheric budget. It is not known how much of the initial Martian atmosphere was left by the end of the Noachian (estimates range from ~ 0.1 bar to 1 bar; Catling, 2014), and how much CO_2 had by then already been stored in crustal sinks, though it is clear that the overall trend since has been one of thinning of the atmosphere to the present-day global value of ~ 6 mbar of pressure. If the massive CO_2 ice deposits (Phillips et al., 2011) were to sublimate, they would add to the atmosphere as much as ~0.006 bar of CO_2 (Bierson et al., 2016). Further compounding the contribution (however small) of putative additional reservoirs of CO_2 ice hidden in the SPLD, could potentially impact estimates of the planetary CO_2 budget.

Here, we present the results of our comprehensive testing of model simulations against the database of MARSIS data acquired over more than 10 years of surveys of the south polar region. We modeled the propagation behaviour of electromagnetic waves at MARSIS operating frequencies (1.8-5 MHz) under a variety of conditions involving different configurations of thin layers of solid CO_2, H_2O ice and dust. Within the parameter space we explored, the models do not return values of reflection consistent with the observed MARSIS data. We thus reject the notion that the bright basal reflections detected at Ultimi Scopuli may indicate the presence of thin layers of CO_2-ice at the base of the SPLD.

2. Geological Setting

The South Polar Layered Deposits (SPLD), covering most of the Planum Australe of Mars (Fig. 1), form an up to 3.7 km thick (Plaut et al., 2007) stratified unit, composed of pure water ice interlayered with thin dust-rich deposits. It has been estimated that the content of dust in the SPLD is ~ 10-15% (Plaut et al., 2007; Zuber et al., 2007), although inhomogeneities in the values of inverted density of the deposits indicate that the dust is not uniformly distributed (Li et al., 2012), and that the fraction of dust in the water ice would vary depending on the presence of denser CO_2 ice (Broquet et al., 2021). The layers are directly observed in radar imagery where troughs and scarps cut through the deposits (Milkovich and Plaut, 2008). Owing to the electromagnetic contrast between the values of dielectric permittivity ε of ice (3.12; Pettinelli et al., 2015) and dust (> 4; Mattei et al., 2014), layering is also detected by radar sounder observations (Plaut et al., 2006, 2007; Milkovich et al., 2009; Whitten and Campbell, 2018). Layering of the deposits is thought to reflect differential dust and ice accumulation rates influenced by global climate cycles linked to orbital forcing (e.g., Hvidberg et al., 2012). The deposits decrease in elevation and thickness at the margins, eventually waning and revealing underlying Noachian and Hesperian highlands terrains (Tanaka and Kolb, 2001), overlain by a thin mantle of desiccated or water-ice pore-filled soil (Putzig et al., 2005; Jones et al., 2014). The surface age of the SPLD is 7-100 Ma, based on the impact crater record (Herkenhoff and Plaut, 2000; Koutnik et al., 2002). The age of the lowermost strata of the SPLD sequence is presently undetermined. A detailed geological analysis and interpretation of the unconformities observed in Promethei Lingula suggests that the current extent of the SPLD may have started forming no earlier than 250 Ma (Guallini et al., 2018). This estimate is consistent with time-series analysis of HiRISE and CaSSIS stereo-images of the internal structure of the SPLD shown along scarp faces, suggesting that the minimum time of accumulation of the SPLD is 10-30 Myr, resulting in a minimum age of deposition for the basal layers of 17 to 130 Ma (Becerra et al., 2019).

The SPLD have been subdivided into three distinct structures (Milkovich and Plaut, 2008): the *Promethei Lingula Layer* Sequence (PLL), the *Bench Forming Layer* Sequence (BFL), and the *Inferred Layer* Sequence (IL). The BFL is the top sequence, geographically located in the central west-northwest portion of the SPLD, where the deposits measure their highest elevations (~ 3500-4500 m). The BFL is covered by thin layers of CO_2 ice (part of the South Polar Residual Cap, SPRC). Underlying the BFL is the PLL, while IL is inferred to be the basal sequence in the west of the deposits. Elsewhere, only the PLL exists (ref. to figs. 18-19, in Milkovich and Plaut, 2008), its lateral extent corresponding to that of Tanaka et al.'s (2014) *Apu* (Amazonian polar undivided) unit (Fig. 1).

The South Polar Residual Cap (SPRC), which is part of geological unit *lApc* (Fig. 1), straddles the prime meridian, approximately between longitudes 250°E-40°E and latitudes 85-90°S. The cap is primarily composed of a high albedo thin (<10 m) layer of CO_2 ice (Byrne and Ingersoll, 2003), with a characteristic «Swiss cheese» appearance (Malin et al., 2001) due to the presence of pits that reveal underlying water ice (Zuber et al., 2007). Observed constant rates of erosion of the pits (Thomas et al., 2013) have been interpreted to point to net loss of CO_2 from the SPRC, possibly counterbalanced by observed net gain of seasonal water ice (Brown et al., 2014), suggesting orbital effects are responsible for the CO_2 and H_2O atmosphere-SPRC exchanges. Localized deposits up to 1 km thick, formed by alternating layers of CO_2 ice (each approximately 100 m thick) and H_2O ice (a few m thick) have also been detected (Phillips et al., 2011; Bierson et al., 2016) by the radar sounder SHARAD, in troughs and at the base of scarps of the BFL structural unit, to the west of the location of the inferred rim of the ~ 870 km diameter Noachian impact crater Prometheus Basin (Fig. 1). This suggests a possible relationship between the basal topography in this area, and atmospheric conditions that caused deposition of CO_2 ice here. It has been proposed that H_2O ice entombs the CO_2 ice layers, thus isolating them from the atmosphere and preventing their erosion (Manning et al., 2019). An alternative hypothesis argues that the deposits are in communication with the atmosphere, and that variations in polar incident sunlight from Mars's 100 kyr orbital cycles balance the exchange between CO_2 in the deposits and in the atmosphere. The observed deposits should thus record the last 510 kyr of Martian polar climate history (Buhler et al., 2021). Observations by SHARAD and MARSIS radars did not detect CO_2 ice layers anywhere else in the SPLD (Whitten et al., 2017; Whitten and Campbell, 2018; Khuller and Plaut, 2021).

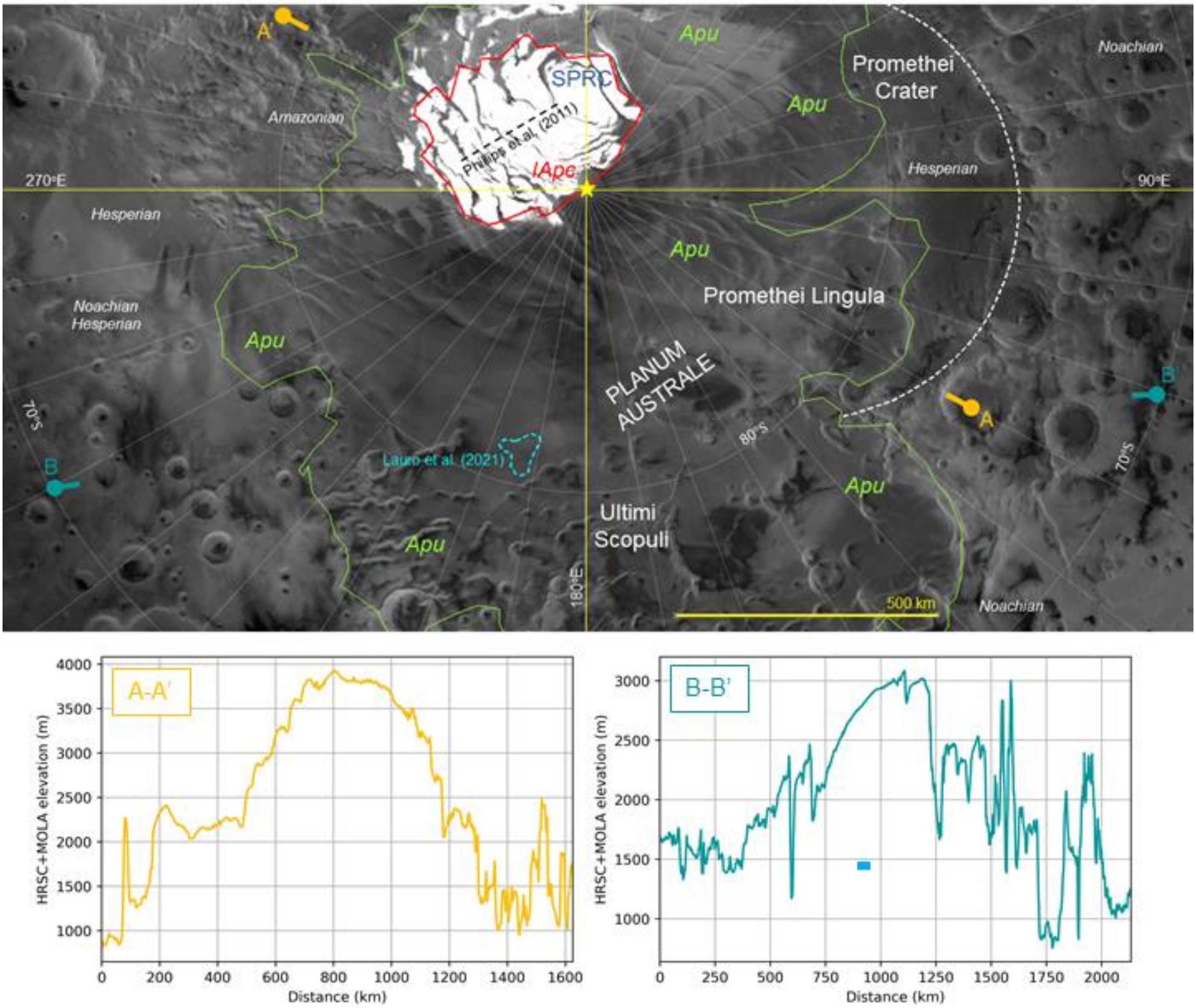

Fig. 1. Context map of the south polar region. The map shows the extent of the geological units and geographic features described in Section 2. The dashed aqua polyline indicates the location of the strong basal reflections detected by Lauro et al. (2021). The trace of the ground track of the tract of SHARAD orbit 5968-01 traversing the RFZ_3 (Phillips et al., 2011) is shown as a black dashed line on the south pole residual cap (SPRC). Yellow star: South Pole. Vertical yellow line: prime and anti- meridians. Dashed white line: approximate position of remnant of rim of Promethei Crater. Lime green polyline: boundary of Amazonian polar undivided unit (*Apu*). Red polyline: boundary of late Amazonian polar cap unit (*lApc*). A-A': end points of topographic profile A-A' (orange). B-B': end points of topographic profile B-B' (green). The short light blue segment in topographic profile B-B' indicates the

position and inferred depth of the bright basal reflections. Elevations are blended DEM/DTM (200 m/pixel) from MOLA and HRSC data. Geological units are described by Tanaka et al. (2014). Geographic grid interval: 10°. Mapped with JMARS.

Ultimi Scopuli is a vast terminal region of the deposits, part of the *Apu* geological unit (Fig. 1) and of the structural PLL sequence. Here, between coordinates 191°E-196°E and 80.3-81.5°S, and at a depth of approximately 1.5 km, recent orbiter sounder MARSIS observations (Orosei et al., 2018a; Lauro et al., 2021) revealed the presence of four high permittivity areas, interpreted to be bodies of basal liquid water. The heat flow at the Martian south polar regions is ~ 22-26 mW/m^2 (Grott et al., 2013; Plesa et al., 2018), and there is presently no evidence of an anomalous geothermal gradient or localized hot spot (such as a magma chamber, as postulated by Sori and Bramson, 2019), that would plausibly increase the basal temperature. The overburden pressure, estimated to be ~ 6 MPa (considering an average density of the SPLD = 1220 kg/m^3, from Zuber et al., 2007, which is the same as the best fit value published by Broquet et al., 2021, and also consistent with a local value of ~ 1200 kg/m^3, as inferred from the inverted density map of the SPLD published by Li et al., 2012), would also be insufficient for ice to melt. Therefore, to explain the presence of basal liquid water, Orosei et al. (2018a) suggested that the water may be a perchlorate brine. Subsequently, Lauro et al. (2021) further defended this interpretation, on the grounds that supercooled perchlorate brines have been shown to form and persist at sub-eutectic temperatures (Toner et al., 2014; Primm et al., 2017), within the range of those reasonably expected at the base of the SPLD. The reflections at the base of Ultimi Scopuli are located over a gently sloping basement (Lauro et al., 2021).

3. Model

3.1. Preliminary Analysis

The fundamental concept underpinning this study is that the electromagnetic waves locally reflected from interfaces between the layers in a stratified structure, can combine to enhance (constructive interference) or suppress (destructive interference) the overall radar response from a layered structure. As a preliminary analysis, we explored the specific parameter space presented by Lalich et al.'s (2021a) model, consisting of a thin layer of pure water ice sandwiched between two thin layers of CO_2 ice: thus, we modelled the variation of only three parameters, i.e., the thickness of each of the three layers. Layer thicknesses greater than a few tens of m dampen resonance effects, because longer propagation paths decrease the likelihood of simultaneous in-phase sum of sinusoids at different frequencies (Supplementary Figure 5, Orosei et al., 2018a). Therefore, we constrained the simulated thickness of each layer to be $\leq$ 100 m. In the field of numerical electromagnetic modelling, spatial discretization is usually set to be less than 1/10 of the wavelength. The shortest wavelength transmitted by MARSIS is 30 m in water ice. Thus, we applied simulated thickness increments of 1 m as our sampling interval, to obtain accurate model stratigraphy responses to the MARSIS pulses. We ran more than one million simulations (101 × 101 × 101) at MARSIS operating frequencies of 3, 4 and 5 MHz, obtaining a complete characterization of the properties of Lalich et al.'s (2021a) model.

The highest value of subsurface-to-surface echo power ratio we obtained was 4.7 dB. Because the radar response to the stratigraphy is described by sinusoidal functions, we ruled out the eventuality that we might have missed peaks in the subsurface echo: considering that variations in the radar response between consecutive data points are negligible (a fraction of a decibel at most), the model stratigraphy subsurface-to-surface echo power ratios would never exceed ~ 5 dB, even in the case that the position of our maxima were not exact.

For each frequency, we obtained five well-defined regions in parameter space with subsurface-to-surface radar echo power ratio values > 4 dB (Fig. 2). These regions are specific to each frequency, because constructive interference phenomena are primarily controlled by layer thickness / wavelength ratios. Consequently, while basal echo powers remain high for small variations of thickness around the local maxima at one frequency, the corresponding echo powers at the other two frequencies are lower and much more widely dispersed (Fig. 3). Thus, if we take the parameter values corresponding to the maxima found at one frequency as a reference, and calculate the subsurface-to-surface echo power ratio differences between this frequency and the other two, these will always favour the reference frequency (Fig. 4).

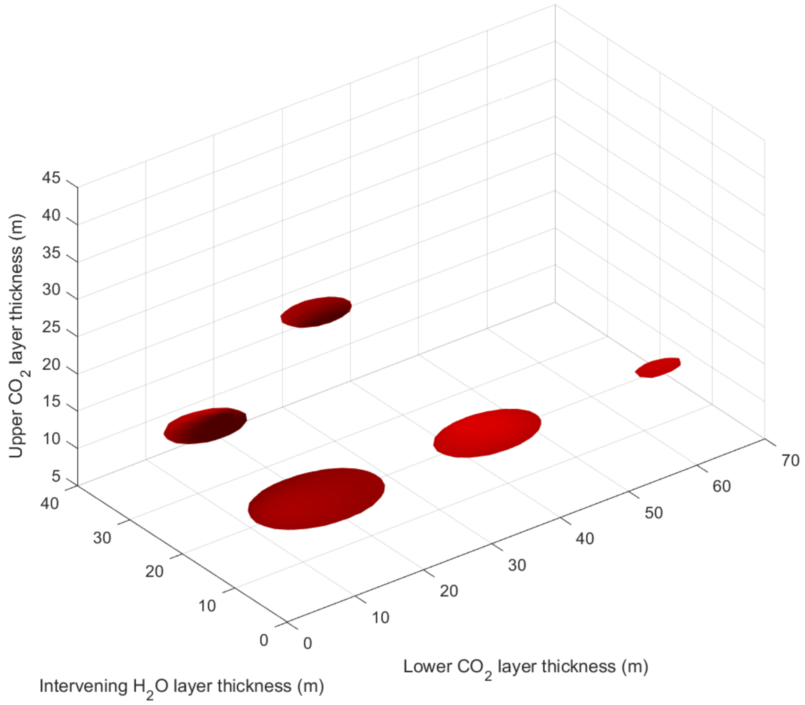

Fig. 2. Location of strong basal echoes (> 4 dB greater than surface echoes) produced in simulations at 4 MHz, displayed in the parameter space of the model by Lalich et al. (2021a), consisting of three quantities, specifically: the thickness of two CO_2 layers, and of a pure water ice layer sandwiched between them. Simulations at 3 and 5 MHz produce the same pattern, but with local maxima in different positions.

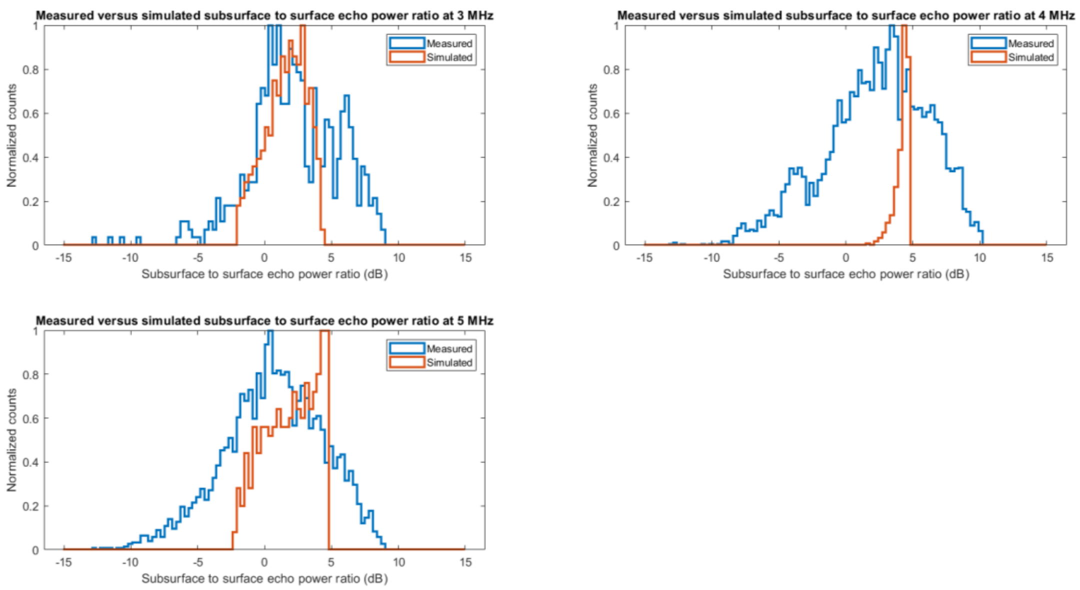

Fig. 3. Histograms of subsurface-to-surface echo power ratios obtained for simulations (orange) with a bottom CO_2 ice layer of thickness ranging between 8 m and 14 m, a top CO_2 ice layer 9-15 m thick, and an interbedded H_2O ice layer 9-15 m thick. Blue histograms represent real MARSIS observations.

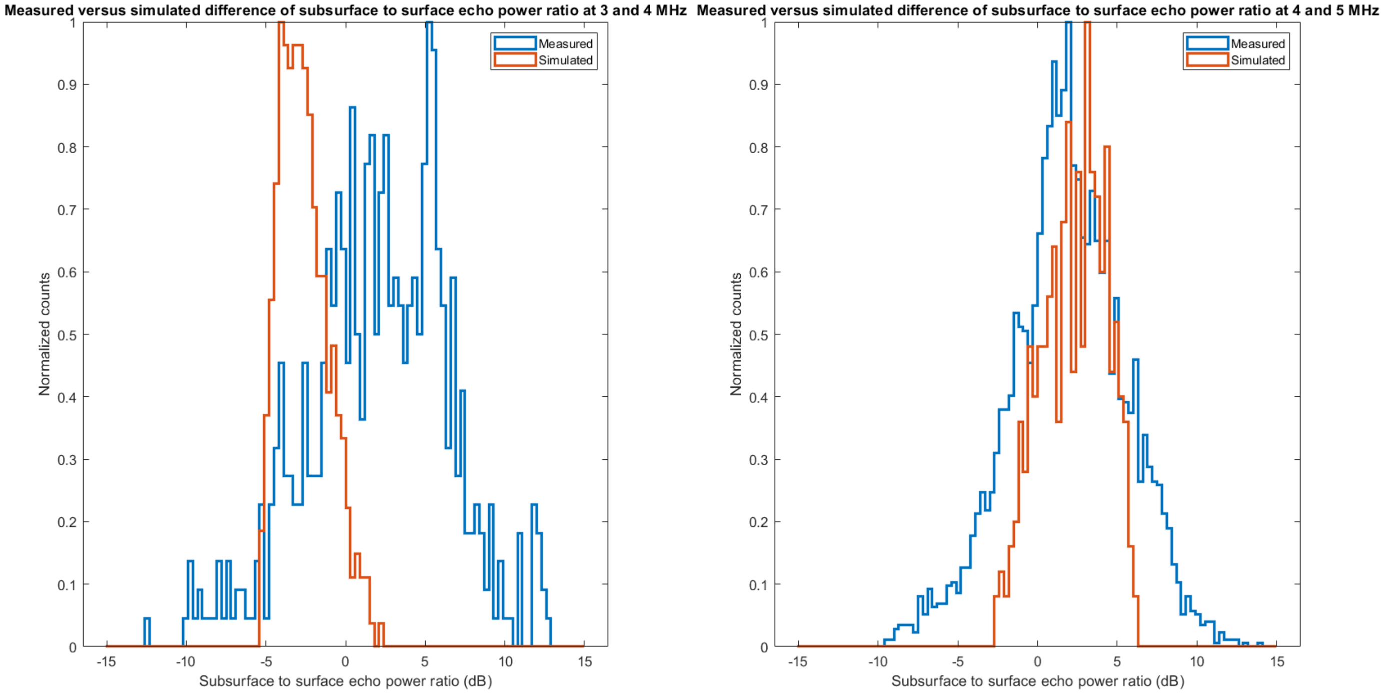

Fig. 4. Histograms of basal-to-surface echo power ratio differences between pairs of MARSIS operating frequencies (3 and 4 MHz, and 4 and 5 MHz). Simulation conditions are the same as for those in Fig. 3. Blue histograms are for real MARSIS observations.

Our preliminary analysis indicates that the distribution and behavior of subsurface-to-surface echo power ratios simulated in the parameter space as described, contrast sharply with that of real MARSIS data. However, idealized models do not consider possible sources of echo power fluctuations that affect real data, and thus some discussion is needed before a comparison between data and model is attempted.

The model used and discussed by Orosei et al. (2018) is computationally the same used by Lalich et al. (2021a, 2021b), that is the one-dimensional solution of Maxwell equations in a plane parallel stratigraphy. The former model had a simpler stratigraphy compared to the latter, with the SPLD represented as a single homogeneous layer composed of a mixture of H_2O ice and dust. The model was run varying basal temperature, dust content and basal permittivity. These three parameters controlled the attenuation within the SPLD and the intensity of the reflection at the bottom of the SPLD. The results showed that even for low amounts of dust and basal temperatures, it was necessary to have a high basal reflectivity to produce the observed strong basal echoes.

The model parameters published by Lalich et al. (2021b) are exactly the same, except for the input of single values for dust fraction, basal temperature and basal permittivity. These authors varied the thickness of the layers at the base of the SPLD.

Because of the similarity of the mathematical formulation of the two models, we compared them directly to one another to assess their capability to reproduce MARSIS observations, following the same approach used by Lalich et al. (2021b). For example, Figure 3 in that paper shows reflections produced by a single CO_2 layer model that are as strong as the ones observed by MARSIS, although the authors neglected to specify that their reference values for MARSIS echo power are the medians of observed values, and that normalized echo power can reach values as high as 10 dB (see Figure 4 and S4 in Orosei et al., 2018), well above any value that can be obtained by the single layer model shown in Figure 3.

The capability of the model in Orosei et al. (2018) to produce strong echoes is thus not due to a more complex mathematical implementation or to a greater number of parameters, but to the fact that basal permittivity can have higher values than those considered by Lalich et al. (2021a, 2021b). In fact, Orosei et al.'s (2018) model could produce basal echoes spanning the full range of observed values (see their Figures 4 and S4), whereas Lalich et al.'s (2021a, 2021b) resulted only in a few instances of basal echo power comparable to observations. The purpose of the present work is therefore to establish the conditions (if these exist), by which Lalich et al.'s (2021) model reproduces the strong radar echoes reported by Orosei et al. (2018). We thus performed comprehensive simulations based on the same mathematics, using a range of possible parameters beyond that explored in that earlier work.

In the following sections, we discuss the sources of variability and error affecting MARSIS observations, evaluating their effect to derive a model of the uncertainties that can be applied to model results, for a more realistic comparison between simulations and data.

3.2 Idealized vs. actual SPLD surface geometry

The assumption of a perfectly flat surface does not prevent the possibility of a comparison with real data, as already shown by Orosei et al. (2018). Furthermore, the subsurface echo power for a given orbit is always normalized to its median value, in order to prevent local minima of surface echo power from producing unrealistically high normalized subsurface echo power values. The choice of using surface median power implies the assumption that the SPLD surface is locally homogeneous, and that surface echo power fluctuations are due to small perturbations of this assumed homogeneity.

To verify if this assumption holds, we need to examine the properties of echo power measured by MARSIS. To this end, we retrieved the same data employed to produce Figure 2 in Orosei et al. (2018) and made publicly available at the time of publication of that paper (Orosei and Cicchetti, 2018). We also produced a simulation of surface echo power similar to those presented and discussed in Orosei et al. (2015). Simulations are used to validate subsurface echo detection by visual comparison: all features present in both the real and simulated radargrams are interpreted as surface clutter, and are therefore excluded from interpretation. A comparison between measurements and simulations for orbit 10737 is shown in Figure 5.

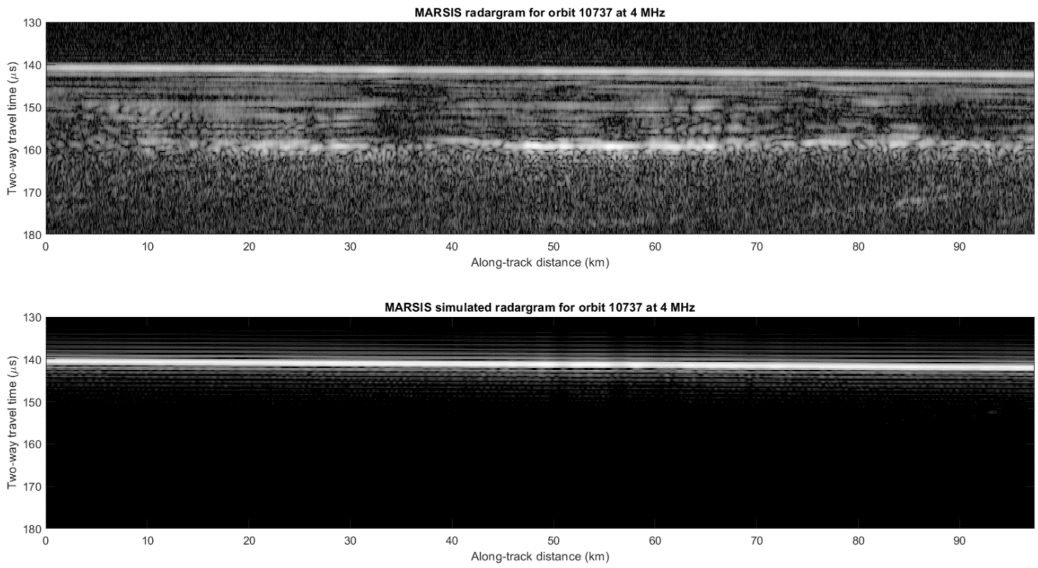

Fig. 5. Top: MARSIS radargram for orbit 10737 at 4 MHz, redrawn following Orosei et al. (2018), versus the corresponding simulation of surface scattering produced using the MOLA topographic dataset (bottom).

The simulated radargram allows also to estimate surface power fluctuations due to surface roughness alone, sampled at the resolution of the MOLA topographic dataset. A comparison with the measured surface power (both arbitrarily normalized to a 0 dB median power for ease of comparison) is shown in Figure 6: it is clear that surface roughness alone accounts for the surface echo power fluctuations at distances between 50 and 60 km along track, which correspond to the location of the bright subsurface reflector.

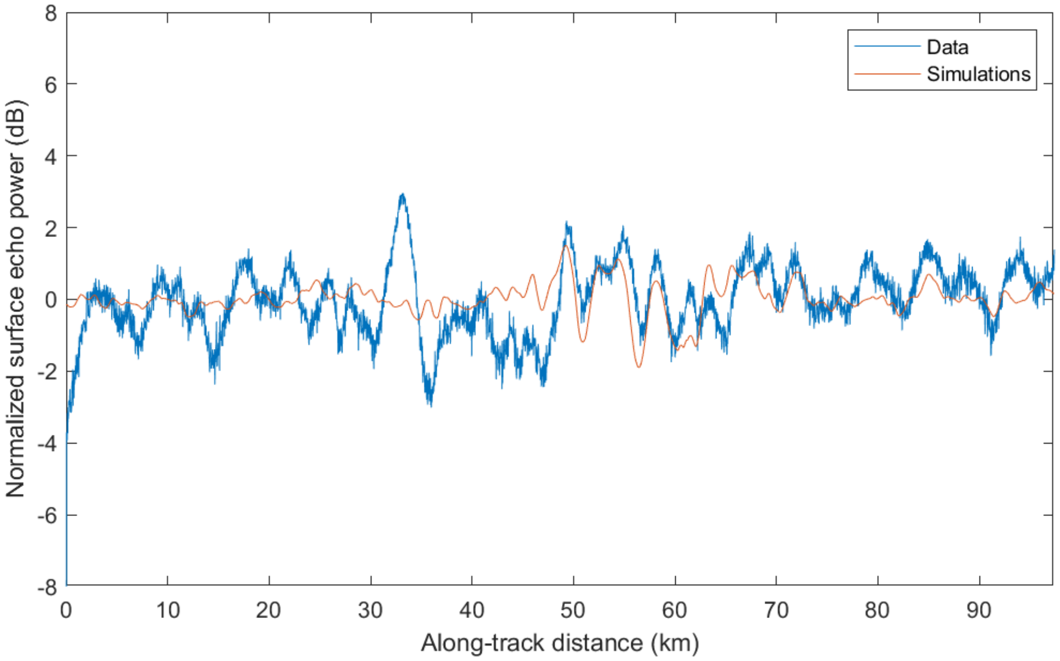

Fig. 6. Measured vs. simulated surface echo power for orbit 10737 at 4 MHz, both arbitrarily normalized to a 0 dB median power for ease of comparison.

The residual difference between data and simulations can be attributed to several factors, such as: surface roughness at scales below MOLA resolution or variations in near-surface density and composition, but the exact cause is difficult to ascertain with available data. Residual power fluctuations are found to have a standard deviation of less than 1 dB, corresponding to a fluctuation of 0.5 in the value of the relative dielectric constant in the assumption that its median value is comprised between 3 and 4 (typical of SPLD materials). Because of the small uncertainties resulting from this analysis, we consider the ratioing with the median surface power as a reasonable calibration method for subsurface echo power.

Furthermore, a previous analysis of SHARAD echoes by Grima et al. (2012) over this area (called Reference Zone or RZ in the paper because of its flatness) showed that surface reflections are predominantly coherent, implying that scattering is near-specular and thus approximates that of a plane surface. This conclusion is even truer at MARSIS wavelength, as the effect of roughness on scattering does not depend on RMS topographic height, but rather on the ratio between RMS topographic height and the wavelength.

It could be argued that even a small roughness causes a decrease (however small) of the mean power of surface echoes, leading to an overestimation of the subsurface-to-surface echo power ratio. In fact, the opposite is true: electromagnetic models and three-dimensional propagation simulations (e.g., Jonard et al., 2019) demonstrate that the wavefront of the radar pulse penetrating through the subsurface is disrupted more than the echo backscattered at the surface, because it crosses the rough surface twice. Thus, the subsurface to surface echo power ratio calculated assuming no surface roughness effect, should be considered a minimum value, with the real ratio likely higher.

3.3 Signal distortion and noise

The MARSIS pulse is not an ideal chirp. Its actual shape and power are unknown: in fact, the spectra reported by Jordan et al. (2009) do not include the frequency-dependent effects of antenna gain, because these could not be measured on ground owing to the length of the antenna. A test comparing the results obtained using Jordan et al.'s (2009) chirp spectra with those obtained using the ideal chirp, does not demonstrate any significant difference. Therefore, the MARSIS data have been range-compressed using an ideal chirp since the beginning of the mission. The range compression is not optimal, with both resolution and signal-to-noise ratio affected. This, however, does not affect the ratio of subsurface to surface echo power. In an abstract mathematical representation, radar sounding can be described as the convolution of the radar waveform with the ideal electromagnetic response of the observed scene. In Fourier transform terms, this convolution is the multiplication of the stratigraphy spectral response with a band-limited signal spectrum, which clips the spectral response bandwidth and produces a limited resolution time-domain response. All these mathematical operations are linear, so the shape of the pulse spectrum will change the power level of echoes from two different interfaces, but not their ratio, which is the quantity used in this analysis.

A few available data also point to a possible dependence of gain on temperature, although a full characterization of this effect was never performed, because it was considered to be negligible under the conditions at which MARSIS acquires its observations. Furthermore, MARSIS raw data takes are at most 25 seconds long, which is too short a time to produce any significant gain variation. This is further corroborated by the plot of surface echo power shown in Figure 6, which does not show any trend of varying gain across the entire observation. Thus, within the limits of what it is technically possible to ascertain about the causes and extent of non-ideality of range compression in MARSIS, there is no effect that should be considered as introducing a bias in the use of median surface echo power as a calibration reference for subsurface echo power.

Plots of the noise level in the observations (Orosei and Cicchetti, 2018) analysed by Orosei et al. (2018) show constant noise level across a single observation, and nearly-constant noise levels across observations at the same frequency (around -5 dB at 3 and 4 MHz and -11 dB at 5 MHz when expressed in uncalibrated digital numbers). The median signal-to-noise ratio is > 20 dB for all observations, exceeding 30 dB.

Interferences caused by the electronics of the Mars Express spacecraft were characterized in the commissioning phase of MARSIS. Limited available documentation shows a correlation with the activity of the HRSC camera, though no systematic analysis has ever been published. Overall, data acquired over the lifetime of the mission show that the combined electromagnetic interferences (EMI) caused by orbiter navigation and experiment instrumentations, have a much smaller effect on the functioning of MARSIS than (for example) on its Mars Reconnaissance Orbiter companion SHARAD. Thus, the operating assumption is that EMI have a negligible effect on the subsurface to surface echo power ratio.

The MARSIS data analyzed by Orosei et al. (2018) consist of near-simultaneous observations at two frequencies, namely 3 and 4 MHz, or 4 and 5 MHz. Thus, it is possible to compute the subsurface to surface echo power ratio at two frequencies for the same observation. Doing so for data in which surface echo power has a standard deviation below 1 dB (as noted in Table S1 in the Supplementary Materials of Orosei et al., 2018), one is left only with data at 4 and 5 MHz. The difference between normalized power at those two frequencies has a median value of 1.36 dB, which can be used for a back-of the envelope computation based on equations found in Porcello et al. (1974) to obtain an estimate of the loss tangent (see also Orosei et al., 2020 for the effect of such loss tangent value on SHARAD measurements). The resulting value is approximately 0.03, which is about fifteen times greater than the one used by Lalich et al. (2021b). Because this value is affected by a large error (the standard deviation of the difference between normalized power at the two frequencies is almost 4 dB), we did not use the estimated loss tangent in simulations. Instead, we considered a variable attenuation as one of the factors decreasing the measured ratio between subsurface and surface power produced by a model.

3.4 Other factors affecting subsurface to surface echo power ratio

Factors affecting subsurface echo power not included in Orosei et al.'s (2018) models are: surface roughness (as discussed above); subsurface roughness (affecting basal echo intensity only); fraction of the radar footprint covered by the basal reflector (see for example Haynes et al., 2018, for a discussion); signal attenuation within the SPLD due to dielectric losses (as discussed above); signal attenuation within the SPLD due to reflection losses in the thinly layered stratigraphy (see for example Courville et al., 2021, for a detailed modelling of propagation in a layered medium at SHARAD frequencies). Their combined effect is demonstrated by the large dispersion of values observed (Figure 7).

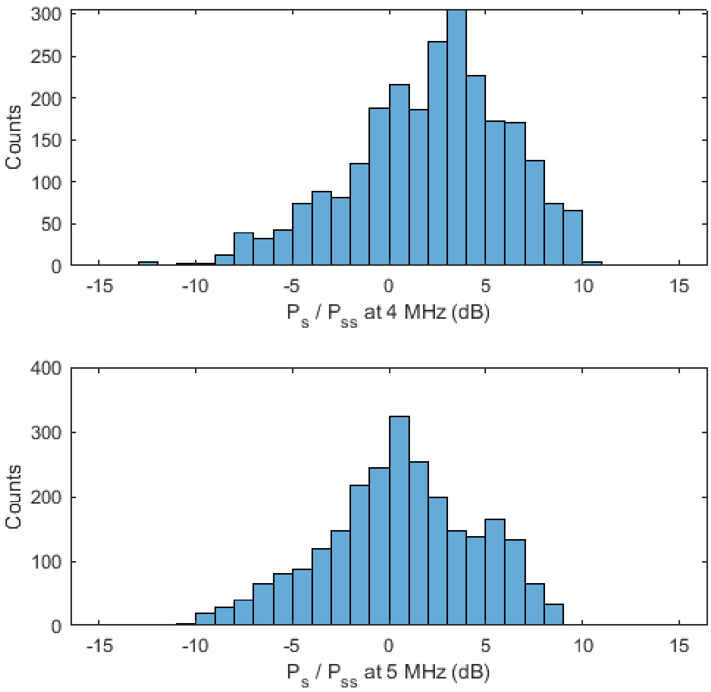

Fig. 7. Histograms of measured values of subsurface to surface echo power ratio over the bright reflector analysed in Orosei et al. (2018) at 4 MHz (top) and 5 MHz (bottom).

The histograms are asymmetric, with a cut-off at high values and a long tail towards low ones. This characteristic matches the intuitive notion that the intensity of a basal reflection cannot increase indefinitely, and would thus have a maximum possible value obtained when all the factors contributing to decreasing basal echo intensity as discussed above are minimized. Thus, a comparison between simulations and data requires the introduction of a model for the random dispersion of measurements. As it is not possible to quantify separately the importance of each factor contributing to basal echo power attenuation, we derived a model probability density function directly from the data (Fig. 8).

The long left-sided tails of the histograms in Figure 7 are characteristic of generalized extreme value distributions, often used to model the maxima of sequences of random variables. Although this is a heuristic method for the selection of the model distribution, it has the merit of matching data histograms better than other parametric distributions.

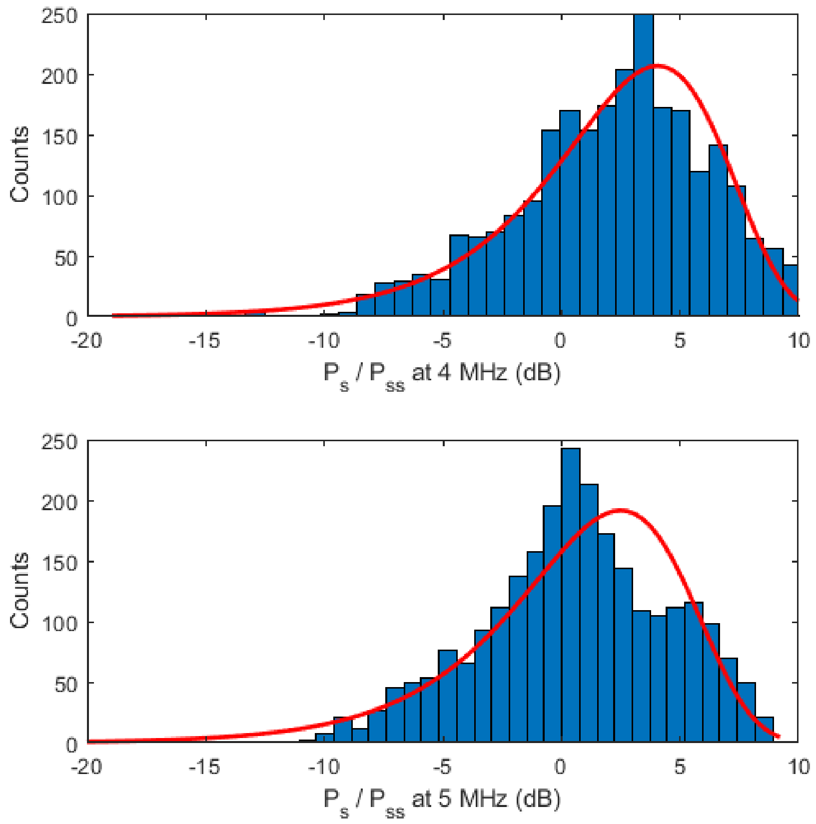

Fig. 8. Best-fit extreme value distributions plotted over the histograms shown in Figure 7.

Through the remainder of this paper, we use these best-fit distributions as the template for randomly generating synthetic measurements from models.

3.5. Electromagnetic propagation model

The propagation of radar waves across stratified media is described by non-linear equations dependent on the electromagnetic properties and thickness of the layers, as well as the probing frequency. Here, we model electromagnetic behaviour of stratified CO_2 ice and dust-laden H_2O ice, by assuming a 1D geometry (Lombardo et al., 2000; Pettinelli et al., 2003; Kartashov et al., 2004; Nunes and Phillips, 2006; Courville et al., 2021). Specifically, we simulate the propagation of radar pulses through twelve idealized models of the SPLD, consisting of sets of perfectly parallel planar interstratified basal layers composed of CO_2 ice and H_2O ice, where the latter has variable contents of dust. The total thickness of the simulated deposits was set at the value derived through MARSIS radargrams over the study area (1.5 km). The material underlying the deposits was set to be basaltic rock. The simulations were run by code adapted from MATLAB$^{(TM)}$ scripts publicly available through a public research data repository (Orosei and Cicchetti, 2018). The code computes the complex reflectivity of the layer stack across the range of frequencies within the pulse bandwidth, multiplying it by the signal spectrum and Inverse-Fourier transforming to the time domain. Simulations were run for one, two or three CO_2 ice layers, the lowermost of which is in direct contact with the bedrock, while the remaining ones are separated by layers of H_2O ice of variable thickness (Fig. 9). CO_2 ice layers are assumed to be lossless.

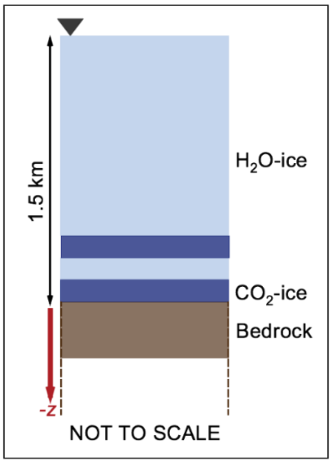

Fig. 9. Schematic stratigraphy used in numerical simulations. The model stratigraphy is here shown as a set of planar parallel layers of CO_2 ice (dark blue) and H_2O ice (light blue), bounded by an upper half space representing the Martian atmosphere (as semi-infinite vacuum) and a lower half space representing the Martian bedrock (brown). Simulations are run for one, two or three lossless CO_2 ice layers, the lowermost of which is in direct contact with the bedrock, while the remaining ones are separated by layers of H_2O ice of variable thickness. The topmost layer of H_2O ice represents the bulk of the stratigraphy. Layer thicknesses of CO_2 ice and interlayer dusty water ice range from 0 to up to 100 m, with total deposit thickness = 1.5 km. The red arrow indicates the depth direction (-*z*). The inverted triangle on top of the sequence indicates the surface of the deposits. The sketch is drawn not to scale.

Typically, complex relative dielectric permittivities are strongly dependent on the frequency of the propagating electromagnetic wave and the temperature of the medium. Attenuation of the signal is independent of frequency at MARSIS wavelength for pure water ice: we used the empirical formulae reported by Mätzler (1998) for the average surface temperature value of 160 K (Clifford, 1987) taken as a constant across the entire model stratigraphy. We find that the real part of the dielectric permittivity of water ice is 3.11, with loss tangent values between $2.5 \cdot 10^{-8}$ (3 MHz) and $3.7 \cdot 10^{-8}$ (5 MHz). The loss tangent of CO_2 ice is not well constrained at the temperature of interest, with extrapolations and upper limits only being reported in the published literature. In our computations therefore, we set it to be = 0, to produce the highest possible subsurface-to-surface echo power ratio values. We did not consider the effect of the complex part of the permittivity of CO_2 on the reflection coefficient, because it is generally assumed to be low ($\leq 10^{-3}$). Computing the Fresnel reflection coefficient at normal incidence for an interface between a layer of CO_2 ice and an underlying bedrock with permittivity values such as those used in the simulations, the results, with and without the inclusion of the imaginary part, differ by < 0.00001.

3.6. Simulations

To calculate the simulated radar waveforms, in our model stratigraphies we assumed perfectly smooth surfaces, an assumption that holds also for small roughness of the illuminated surface, where “small roughness” is defined (Ulaby et al., 1981) by a height < λ /32, which gives a value of 2.35 m at 4MHz. We considered the electromagnetic wave transmitted by the radar having a normal incidence with respect to the model stratified structure (ref. to sketch in Fig. 9), and assumed a 1D-model where the only variation of the electromagnetic properties occurs along the *z*-axis (depth). Furthermore, we assumed spatially homogenous layers with a constant complex dielectric permittivity (ε_i) and thickness (h_i). The stratified structure is bounded by two half-spaces representative of the atmosphere and the bedrock. This model is the same adopted in previous work (Orosei et al., 2018a; Lauro et al., 2019, Lalich et al., 2021a, 2021b). The received signal $y(t)$ is thus computed as:

$$y(t) = \mathcal{F}^{-1}[X(f)R(f)], \qquad (1)$$

where $\mathcal{F}^{-1}$is the inverse Fourier transform, $X(f)$ is the Fourier transform of the signal transmitted by MARSIS antenna, $R(f)$ is the frequency response ($\Gamma_1(f)$) of the layered structure computed from the recursive scattering function $\Gamma_i(f)$:

$$R(f) = \Gamma_1(f)$$
$$\Gamma_i(f) = \frac{\rho_i + \Gamma_{i+1} e^{-2jk_{i+1}h_{i+1}}}{1 + \rho_i \Gamma_{i+1} e^{-2jk_{i+1}h_{i+1}}}, \qquad (3)$$

with k_i the complex-valued wavenumber of the *i*-th layer, and ρ_i the Fresnel reflection coefficient at the boundary between layer *i*–1 and *i*, given by:

$$\rho_i = \frac{\sqrt{\varepsilon_{i-1}} - \sqrt{\varepsilon_i}}{\sqrt{\varepsilon_{i-1}} + \sqrt{\varepsilon_i}}, \qquad (4)$$

The geometry of the problem is modelled as a layered structure, where the upper and lower half space are the same for each simulation, whereas the assumed stratified layer between the atmosphere and the bedrock changes on the basis of the number of CO_2 ice layers, and the thickness of the layers. The ratio between basal and surface power is determined by considering the ratio between the maximum of the square amplitude of $y(t)$ at a time interval containing the echo return from the surface, and that occurring at a time interval containing the echo return from the upper side of the shallower CO_2 ice layer.

Using a multiprocessor machine, we simulated the three CO_2 layer model for every layer thickness between 0 and 50 m at 1-m intervals for three CO_2 layers and two intervening H_2O layers, for a total of 51^5 simulations. This allowed us to sample completely the parameter space of the models with two- and three-basal CO_2 layers, and thus to locate and explore the properties of local maxima embedded in the three- and five-parameter spaces respectively. We identified local maxima of subsurface to surface power ratio, both at 4 and 5 MHz, and for each of them we extracted the basal echo power ratio for all simulations whose layers are within 2 m of the thickness of those corresponding to the local maximum, thus simulating the effect of random but limited variation of the stratigraphy.

4. Results

To implement a quantitative comparison between data and simulation results, for each local maximum of subsurface to surface echo power ratio we produced the histogram of power values extracted from its neighbourhood, and convolved it with the template distributions shown in Figure 8, obtaining a simulated histogram which represents the global effect of the factors affecting propagation within the SPLD on model results. An example of a synthetic distribution is shown in Figure 10.

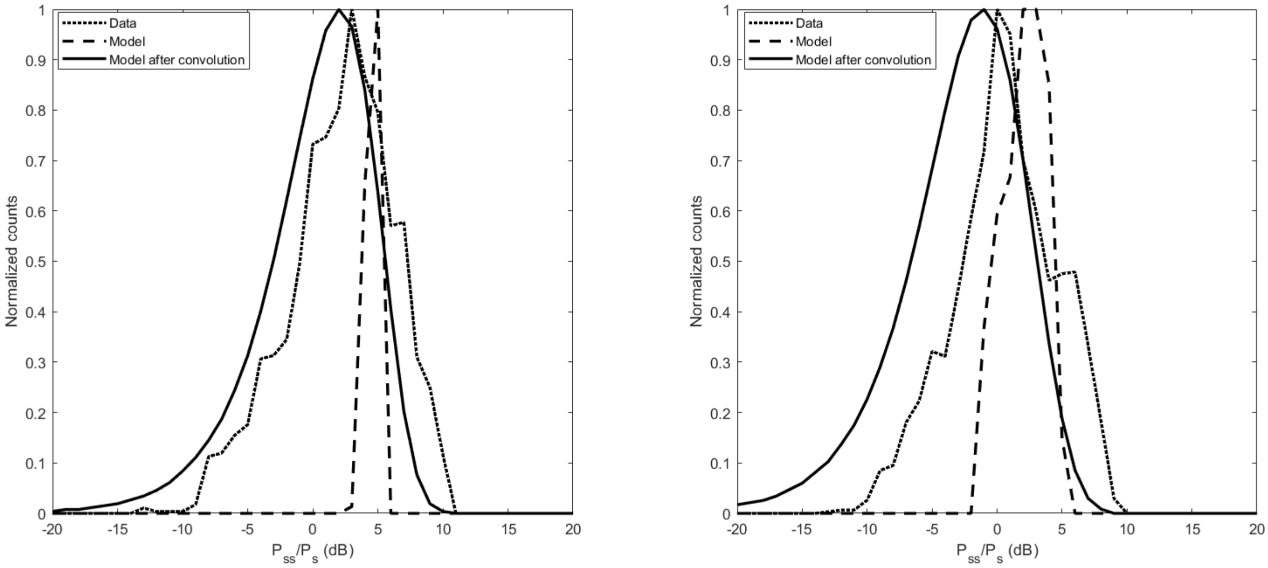

Fig. 10. Comparison between the histogram of measured values of subsurface to surface echo power ratio at 4 (left) and 5 MHz (right) with the histogram of model results in the neighbourhood of a given local maximum (see text for details), and with the synthetic histogram of model results produced through the convolution of the histogram of model results with the distribution template shown in Figure 8. The histograms are computed both for model results at 4 and 5 MHz.

To make a quantitative comparison of model results with data, the synthetic histograms were used to generate a set of random values representing measurements. This was done by taking each histogram bin, and generating a set of uniformly distributed random numbers in an interval corresponding to the bin, whose quantity is proportional to the bin height. Finally, the set of synthetic measurements was compared to actual measurements through a statistical test to determine if the two sets of samples could be produced by the same distribution. We used the two-sample Kolmogorov-Smirnov test (Kolmogorov, 1933; Smirnov, 1939), which is a nonparametric test for the null hypothesis that the data in two sets of samples are from the same continuous distribution. It is widely employed in statistics for its robustness and its sensitivity to both location and shape of distributions. The test was performed using the implementation available in the MATLAB(TM) proprietary programming language, and setting the significance level for the rejection of the null hypothesis at 5%.

A configuration of layers producing a local maximum at one frequency does not result in a local maximum at the other frequency. For this reason, both local maxima at 4 MHz and at 5 MHz had to be considered. Thus, for a given model (either two- or three-CO_2 ice layers) we simultaneously tested samples of model results at 4 and 5 MHz extracted for a set of layer thicknesses corresponding to a local peak of basal echo power at either 4 or 5 MHz, and for all layer thicknesses within two meters of the one producing the peak. This resulted in four possible combinations of number of layers and frequency of the echo power maximum. We found and tested 487 local maxima at 4 MHz and 687 at 5 MHz for the two-layer model, and 2981 local maxima at 4 MHz and 5232 at 5 MHz for the three-layer model. Results are shown in Figure 11.

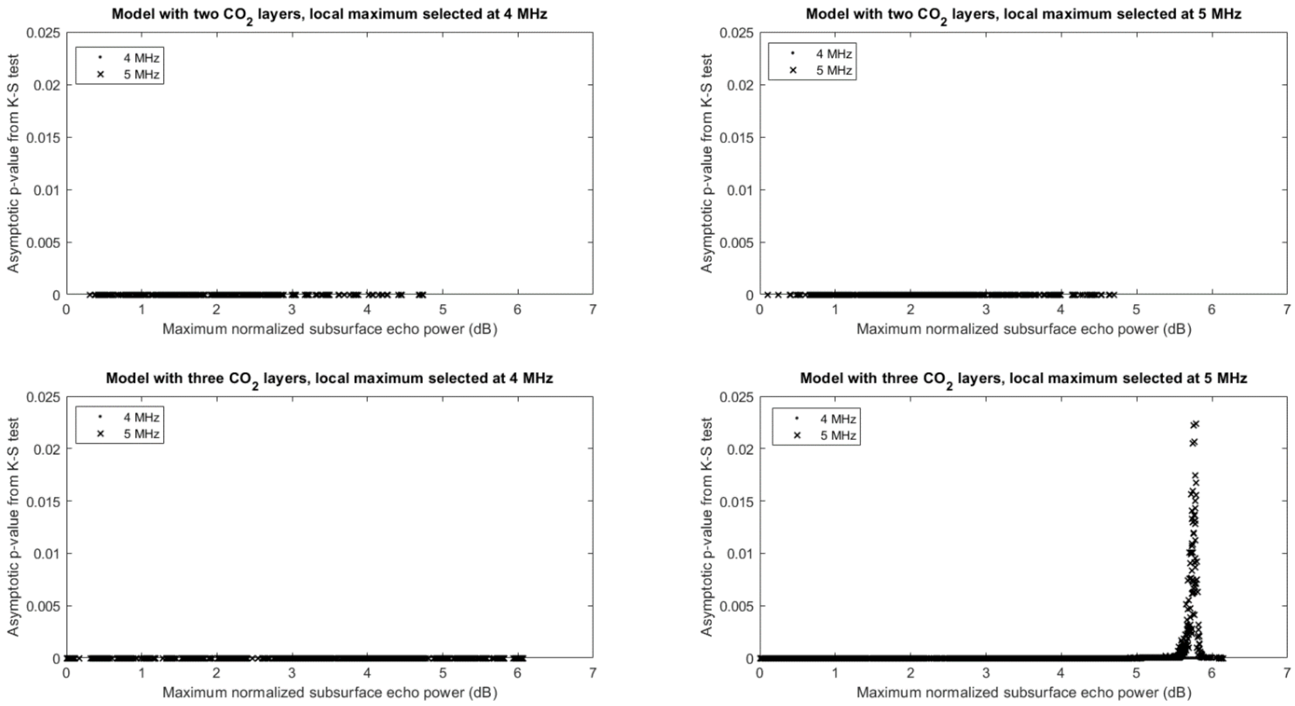

Fig. 11. Plots of the asymptotic p-values produced by the Kolmogorov-Smirnov test versus the maximum subsurface to surface power ratio of simulated echoes, for models with two- and three-CO_2 ice layers and for local maxima at 4 and 5 MHz. Each point represents the probability that model results and MARSIS measurements belong to the same continuous distribution. For each tested set of simulations, probabilities are computed both at 4 MHz (dots) and at 5 MHz (crosses).

No set of two- and three-layer models resulted in simulated values exceeding the 5% significance level threshold. However, it can be seen in the bottom right plot in Figure 11 that a few layer configurations resulting in a local maximum of basal echo power at 5 MHz approach the 5% threshold. This happens only at 5 MHz (crosses in Fig. 11), while at 4 MHz (dots) the probability remains negligible. This quantitatively confirms the observation that, in a model based on the coherent interference between layers, a configuration capable of producing a constructive interference at one frequency is not capable of doing the same at another frequency.

None of the modelled scenarios involving CO_2 ice layers reproduce the distribution of basal echo intensities observed by MARSIS over the bright areas in Ultimi Scopuli. Median values of the simulated basal echo power are lower than those observed in real MARSIS data, and the spread of the simulated values does not match the range of the measured data. We thus conclude that the interpretation that best reconciles all radar observations in Ultimi Scopuli remains that of a strong basal reflector overlain by a thick dust-laden SPLD.

5. Conclusions

The results of our simulations do not support claims that CO_2 ice layers interbedded with water ice can produce the bright reflections detected by MARSIS from the base of the SPLD in Ultimi Scopuli. Therefore, we rule out the presence of hidden deposits of basal CO_2 ice in this area. Based on these results, and the lack of detection of sequestered CO_2 ice deposits elsewhere in the SPLD (Whitten et al., 2017; Whitten and Campbell, 2018; Khuller and Plaut, 2021) beyond those reported by Phillips et al. (2011) and Bierson et al. (2016), we posit that it is unlikely that hidden CO_2 was stored in the late Amazonian (< 250 Ma) south polar deposits. This conclusion is consistent with the geological record of diminishing volcanic activity on Mars during the Hesperian and throughout the Amazonian, with very small amounts of CO_2 released into the atmosphere by volcanic degassing in post-Noachian times.

With the polar caps being the most voluminous reservoir of volatiles on Mars, and their role in regulating the planetary climate, records of the composition and physical properties of the polar layered deposits are fundamental to constrain the entire geological and climatological history of Mars. The ground penetrating radar MARSIS continuing acquisition of observations over the polar regions is an essential element of our investigations into the origin, evolution, and inventory of Martian volatiles and of the planet evolution. This is why interpretations of MARSIS data must be critically assessed against the framework of the physical theory of the propagation of radar waves through stratified media, as we have demonstrated in this paper. Rigorous application of this approach to all investigations based on MARSIS data will advance our knowledge of the nature and properties of Mars's polar materials.

Acknowledgments

The authors are grateful to A.P. Rossi and L. Guallini for their helpful comments on an earlier version of this manuscript. We thank two anonymous reviewers for their constructive criticism and insights, that contributed to clarify and improve the paper. This work was supported by the Italian Space Agency (ASI) through contract ASI-INAF 2019–21-HH.0.

References

Baker, V.R., 2001. Water and the martian landscape. Nature 412, 228-236 https://doi.org/10.1038/35084172.

Baker, V.R., Strom, R., Gulick, V., Kargel, J.S., Komatsu, G., Kale, V.S., 1991. Ancient oceans, ice sheets and the hydrological cycle on Mars. Nature 352, 589-5994 https://doi.org/10.1038/352589a0.

Becerra, P., Sori, M.M., Thomas, N., Pommerol, A., Simioni, E., Sutton, S.S., Tulyakov, S., Cremonese, G., 2019. Timescales of the climate record in the south polar ice cap of Mars. Geophys. Res. Lett. 46 (13), 7268-7277 https://doi.org/10.1029/2019GL083588.

Bierson, C.J., Phillips, R.J., Smith, I.B., Wood, S.E., Putzig, N.E., Nunes, D., Byrne, S., 2016. Stratigraphy and evolution of the buried CO_2 deposit in the Martian south polar cap. Geophys. Res. Lett. 43, 4172-4179 https://doi.org/10.1002/2016GL068457.

Bierson, C.J., Tulaczyk, S., Courville, S.W., Putzig, N.E., 2021. Strong MARSIS radar reflections from the base of Martian south polar cap may be due to conductive ice or minerals. Geophys. Res. Lett. 48(13), e2021GL093880 https://doi.org/10.1029/2021GL093880.

Bridges, J.C., Hicks, L.J., Treiman, A.H., 2019. Carbonates on Mars. In: Filiberto, J. & Schwenzer, S.P. (Eds.) Volatiles in the Martian Crust, pp 89-118 http://dx.doi.org/10.1016/B978-0-12-804191-8.00005-2.

Broquet, A., Wieczorek, M.A., Fa, W., 2021. The composition of the south polar cap of Mars derived from orbital data. J. Geophys. Res. Planets 126(8), e2020JE006730 https://doi.org/10.1029/2020JE006730.

Brown, A.J., Piqueux, S., Titus, T.N., 2014. Interannual observations and quantification of summertime H_2O ice deposition on the Martian CO_2 ice south polar cap. Earth Planet. Sci. Lett. 406, 102-109 http://dx.doi.org/10.1016/j.epsl.2014.08.039.

Buhler, P.B., Ingersoll, A.P., Piqueaux, S., Ehlmann, B.L., Hayne, P.O., 2021. Coevolution of Mars's atmosphere and massive south polar CO_2 ice deposit. Nature Astronomy 4, 363-371 https://doi.org/10.1038/s41550-019-0976-8.

Byrne, S., Ingersoll, A.P., 2003. A sublimation model for Martian south polar ice features. Science 299, 1051-1053 http://science.sciencemag.org/content/299/5609/1051.

Catling, D.C., 2014. Mars atmosphere: History and surface interactions. In: Spohn et al. (Eds.) Encyclopedia of the Solar System, ch. 16, pp. 343- 357 http://dx.doi.org/10.1016/B978-0-12-415845-0.00016-5.

Clifford, S.M., 1987. Polar basal melting on Mars. J. Geophys. Res. 92 (B9), 9135-9152 https://doi.org/10.1029/JB092iB09p09135.

Courville, S.W., Perry, M.R., Putzig, N.E., 2021. Lower bounds on the thickness and dust content of layers within the North Polar Layered Deposits of Mars from radar forward modelling. Planet. Sci. J. 2, 28 https://doi.org/10.3847/PSJ/abda50.

Edwards, C.S., Ehlmann B.L., 2015. Carbon sequestration on Mars. Geology 43(1), 863-866 https://doi.org/10.1130/G36983.1.

Forget, F., Wordsworth, R., Millour, E., Madeleine, J.-B., Kerber, L., Leconte, J., Marcq, E., Haberle, R.M., 2013. 3D modelling of the early martian climate under a denser CO_2 atmosphere: Temperatures and CO_2 ice clouds. Icarus 222, 81-99 http://dx.doi.org/10.1016/j.icarus.2012.10.019.

Grima, C., Kofman, W., Herique, A., Orosei, R., Seu, R. 2012. Quantitative analysis of Mars surface radar reflectivity at 20 MHz. Icarus 220, 84–99. doi:10.1016/j.icarus.2012.04.017

Grott, M., Baratoux, D., Hauber, E., Sautter, V., Mustard, J., Gasnault, O., Ruff, S.W., Karato, S.-I., Debaille, V., Knapmeyer, M., Sohl, F., Van Hoolst, T., Breuer, D., Morschhauser, A., Toplis, M.J., 2013. Long-term evolution of the Martian crust-mantle system. Space Sci. Rev. 174, 49-111 https://doi.org/10.1007/s11214-012-9948-3.

Grott, M., Morschhauser, A., Breuer, D., Hauber, E., 2011. Volcanic outgassing of CO_2 and H_2O on Mars. Earth Planet. Sci. Lett. 308 (3-4), 391-400 https://doi.org/10.1016/j.epsl.2011.06.014.

Guallini, L., Rossi, A.P., Forget, F., Marinangeli, L., Lauro, S.E., Pettinelli, E., Seu, R., Thomas, N., 2018. Regional stratigraphy of the south polar layered deposits (Promethei Lingula, Mars): “Discontinuity-bounded” units in images and radargrams. Icarus 308, 76-107 http://dx.doi.org/10.1016/j.icarus.2017.08.030.

Gulick, V.C., Baker, V.R., 1989. Fluvial valleys and martian palaeoclimates. Nature 341, 514-516 https://doi.org/10.1038/341514a0.

Haberle, R.M., Tyler, D., McKay, C.P., Davis, W.L., 1994. A model for the evolution of CO_2 on Mars. Icarus 109, 102-120 https://doi.org/10.1006/icar.1994.1079.

Haynes, M. S., Chapin, E., Schroeder, D. M. 2018. Geometric Power Fall-Off in Radar Sounding. IEEE Transactions on Geoscience and Remote Sensing 56, 6571–6585. doi:10.1109/TGRS.2018.2840511

Hecht, M., Fisher, D.A., Catling, D.C., Kounaves, S., 2018. RE: Radar evidence of subglacial liquid water on Mars (Orosei et al.). Science eLetters 15 August 2018 https://science.sciencemag.org/content/361/6401/490/tab-e-letters.

Hecht, M.H., Kounaves, S.P., Quinn, R.C., West, S.J., Young, S.M.M., Ming, D., Catling, D.C., Clark, B.C., Boynton, W.V., Hoffman, J., DeFlores, L.P., Gospodinova, K., Kapit, J., Smith, P.H., 2009. Detection of perchlorate and the soluble chemistry of martian soil at the Phoenix lander site. Science 325 (5936), 64-67 https://doi.org/10.1126/science.1172466.

Herkenhoff, K.E., Plaut, J.J., 2000. Surface ages and resurfacing rates of the polar layered deposits on Mars. Icarus 144, 243-253 https://doi.org/10.1006/icar.1999.6287.

Hvidberg, C.S., Fishbaugh, K.E., Winstrup, M., Svensson, A., Byrne, S., Herkenhoff, K.E., 2012. Reading the climate record of the martian polar layered deposits. Icarus 221 (1), 405-419 https://doi.org/10.1016/j.icarus.2012.08.009.

Jakosky, B.M., 2019. The CO_2 inventory on Mars. Planet. Space Sci. 175, 52-59 https://doi.org/10.1016/j.pss.2019.06.002.

Jakosky, B.M., 2021. Atmospheric loss to space and the history of water on Mars. Annu. Rev. Earth Planet. Sci. 49, 71-93 https://doi.org/10.1146/annurev-earth-062420-052845.

Jakosky, B.M., Henderson, B.G., Mellon, M.T., 1995. Chaotic obliquity and the nature of the Martian climate. J. Geophys. Res. Planets 100, 1579-1584 https://doi.org/10.1029/94JE02801.

Jonard, F., André, F., Pinel, N., Warren, C., Vereecken, H., Lambot, S. 2019. Modeling of Multilayered Media Green’s Functions With Rough Interfaces. IEEE Transactions on Geoscience and Remote Sensing 57, 7671-7681. doi: 10.1109/TGRS.2019.2915676.

Jones, E., Caprarelli, G., Mills, F.P., Doran, B., Clarke, J., 2014. An alternative approach to mapping thermophysical units from Martian thermal inertia and albedo data using a combination of unsupervised classification techniques. Remote Sensing 6, 5184-5237 https://doi.org/10.3390/rs6065184.

Kartashov, D.V., Shchuko, O.B., Orosei, R., 2004. Radar detection of subsurface features on Mars. Advances in Space Research 33 (12), 2263-2269 https://doi.org/10.1016/S0273-1177(03)00525-8.

Kahn, R., 1985. The evolution of CO_2 on Mars. Icarus 62, 175-190 https://doi.org/10.1016/0019-1035(85)90116-2.

Khuller, A.R., Plaut, J.J., 2021. Characteristics of the basal interface of the Martian South Polar Layered Deposits. Geophys. Res. Lett. 38, e2021GL093631 https://doi.org/10.1029/2021GL093631.

Kolmogorov, A. N. 1933. Sulla determinazione empirica di una legge di distribuzione. Giornale dell’Istituto Italiano degli Attuari 4, 83–91.

Koutnik, M., Byrne, S., Murray, B., 2002. South Polar Layered Deposits of Mars: The cratering record. J. Geophys. Res. Planets 107 (E11), 5100, doi: 10.1029/2001JE001805 https://doi.org/10.1029/2001JE001805.

Lalich, D.E., Hayes, A.G., Poggiali, V., 2021a. Explaining bright radar reflections in the Martian SPLD without liquid water. Lunar Planet. Sci. Conf. LII, 2392.

Lalich, D. E., Hayes, A. G., Poggiali, V. 2021b. Explaining Bright Radar Reflections Below The Martian South Polar Layered Deposits Without Liquid Water. arXiv e-prints https://doi.org/10.48550/arXiv.2107.03497

Lauro, S.E., Pettinelli, E., Caprarelli, G., Guallini, L., Rossi, A.P., Mattei, E., Cosciotti, B., Cicchetti, A., Soldovieri, F., Cartacci, M., Di Paolo, F., Noschese, R., Orosei, R., 2021. Multiple subglacial water bodies below the south pole of Mars unveiled by new MARSIS data. Nature Astronomy 5, 63-70 https://doi.org/10.1038/s41550-020-1200-6.

Lauro, S.E., Soldovieri, F., Orosei, R., Cicchetti, A., Cartacci, M., Mattei, E., Cosciotti, B., Di Paolo, F., Noschese, R., Pettinelli, E., 2019. Liquid water detection under the South Polar Layered Deposits of Mars – A probabilistic inversion approach. Remote Sensing 11 (20), 2445 https://doi.org/10.3390/rs11202445.

Li, J., Andrew-Hanna, J.C., Sun, Y., Phillips, R.J., Plaut, J.J., Zuber, M.T., 2012. Density variations within the south polar deposits of Mars. J. Geophys. Res. Planets 117(E4), doi: 10.1029/2011JE003937 https://doi.org/10.1029/2011JE003937.

Lombardo, P., Magenta, A.M., Pettinelli, E., 2000. Multichannel fusion of subsurface radar images at different resolutions. IEE Proc. Radar, Sonar and Navigation 147 (3), 121-133 https://digital-library-theiet.org/content/journals/10.1049/ip-rsn_20000196.

Malin, M.C., Caplinger, M.A., Davis, S.D., 2001. Observational evidence for an active surface reservoir of solid carbon dioxide on Mars. Science 294 (5549), 2146-2148 https://science.sciencemag.org/content/294/5549/2146.

Manning, C.V., Bierson, C., Putzig, N.E., McKay, C.P., 2019. The formation and stability of buried polar CO_2 deposits on Mars. Icarus 317, 509-517 https://doi.org/10.1016/j.icarus.2018.07.021.

Mattei, E., Lauro, S.E., Vannaroni, G., Cosciotti, B., Bella, F., Pettinelli, E., 2014. Dielectric measurements and radar attenuation estimation of ice/basalt sand mixtures as martian Polar Caps analogues. Icarus 229, 428-433 https://doi.org/10.1016/j.icarus.2013.10.017.

Mätzler, C., 1998. Microwave properties of ice and snow. In: Schmitt B, De Bergh C, Festou M (Eds.) Solar System Ices. Astrophys. Space Sci. Library 227, 241-257 https://doi.org/10.1007/978-94-011-5252-5_10.

Mellon, M.T., 1996. Limits on the CO_2 content of the Martian polar deposits. Icarus 124, 268-279 https://doi.org/10.1006/icar.1996.0203.

Mellon, M.T., Feldman, W.C., Prettyman, T.H., 2004. The presence and stability of ground ice in the southern hemisphere of Mars. Icarus 169, 324-340 https://doi.org/10.1016/j.icarus.2003.10.022.

Michalski, J.R., Niles, P.B., 2010. Deep crustal carbonate rocks exposed by meteor impact in Mars. Nature Geoscience 3, 751-755 https://doi.org/10.1038/ngeo971.

Milkovich, S.M., Plaut, J.J., 2008. Martian South Polar Layered Deposit stratigraphy and implications for accumulation history. J. Geophys. Res. Planets 113, E06007, doi: 10.1029/2007JE002987 https://doi.org/10.1029/2007JE002987.

Milkovich, S.M., Plaut, J.J., Safaenili, A., Picardi, G., Seu, R., Phillips, R.J., 2009. Stratigraphy of the Promethei Lingula, south polar layered deposits, Mars, in radar and imaging datasets. J. Geophys. Res. Planets 114, E03002, doi: 10.1029/2008JE003162 https://doi.org/10.1029/2008JE003162.

Nunes, D.C., Phillips, R.J., 2006. Radar surface mapping of the polar layered deposits on Mars. J. Geophys. Res. Planets. 111 (E6), E06S21, doi: 10.1029/2005JE002609 https://doi.org/10.1029/2005JE002609.

Orosei, R., Cicchetti, A., 2018. Data files and electromagnetic simulation software used in the paper “Radar evidence of subglacial liquid water on Mars” by Orosei et al. (2018) [Data set]. Zenodo https://zenodo.org/record/1285179.

Orosei, R., Jordan, R.L., Morgan, D.D., Cartacci, M., Cicchetti, A., Duru, F., Gurnett, D.A., Heggy, E., Kirchner, D.L., Noschese, R., Kofman, W., Masdea, A., Plaut, J.J., Seu, R., Watters, T.R., Picardi, G., 2015. Mars Advanced Radar for Subsurface and Ionospheric Sounding (MARSIS) after nine years of operation: A summary. Planet. Space. Sci. 112, 98-114 https://doi.org/10.1016/j.pss.2014.07.010.

Orosei, R., Lauro, S.E., Pettinelli, E., Cicchetti, A., Coradini, M., Cosciotti, B., Di Paolo, F., Flamini, E., Mattei, E., Pajola, M., Soldovieri, F., Cartacci, M., Cassenti, F., Frigeri, A., Giuppi, S., Martufi, R., Masdea, A., Mitri, G., Nenna, C., Noschese, R., Restano, M., Seu, R., 2018a. Radar evidence of subglacial liquid water on Mars. Science 361 (6401), 490-493 http://science.sciencemag.org/content/361/6401/490.

Orosei, R., Lauro, S.E., Pettinelli, E., Cicchetti, A., Coradini, M., Cosciotti, B., Di Paolo, F., Flamini, E., Mattei, E., Pajola, M., Soldovieri, F., 2018b. RE: Response to Orosei et al., Radar evidence of subglacial liquid water on Mars, by Hecht, Fisher, Catling and Kounaves. Science eLetters 29 August 2018 https://science.sciencemag.org/content/361/6401/490/tab-e-letters.

Orosei, R. and 11 colleagues 2020. The Global Search for Liquid Water on Mars from Orbit: Current and Future Perspectives. Life 10, 120. doi:10.3390/life10080120.

Pestova, O.N., Myun, L.A., Khripun, M.K., Prigaro, A.V., 2005. Polythermal study of the systems $M(ClO_4)_2$-H_2O ($M^{2+} = Mg^{2+}$, Ca^{2+}, Sr^{2+}, Ba^{2+}). Russian J. of Appl. Chemistry 78 (13), 409-413 https://doi.org/10.1007/s11167-005-0306-z.

Pettinelli, E., Cosciotti, B., Di Paolo, F., Lauro, S.E., Mattei, E., Orosei, R., Vannaroni, G., 2015. Dielectric properties of Jovian satellite ice analogs for subsurface radar exploration: A review. Rev. Geophys. 53 (3), 593-641 https://doi.org/10.1002/2014RG000463.

Pettinelli, E., Vannaroni, G., Cereti, A., Paolucci, F., Della Monica, G., Storini, M., Bella, F., 2003. Frequency and time domain permittivity measurements on solid CO_2 and solid CO_2-soil mixtures as Martian soil simulants. J. Geophys. Res. Planets 108 (E4), 8029, doi: 10.1029/2002JE001869 https://doi.org/10.1029/2002JE001869.

Phillips, R.J., Davis, B.J., Tanaka, K.L., Byrne, S., Mellon, M.T., Putzig, N.E., Haberle, R.M., Kahre, M.A., Campbell, B.A., Carter, L.M., Smith, I.B., Holt, J.W., Smrekar, S.E., Nunes, D.C., Plaut, J.J., Egan, A.F., Titus, T.N., Seu, R., 2011. Massive CO_2 ice deposits sequestered in the South Polar Layered Deposits of Mars. Science 332 (6031), 838-841 https://science.sciencemag.org/content/332/6031/838.

Picardi, G., Biccari, D., Seu, R., Marinangeli, L., Johnson, W.T.K., Jordan, R.L., Plaut, J., Safaenili, A., Gurnett, D.A., Ori, G.G., Orosei, R., Calabrese, D., Zampolini, E., 2004. Performance and surface scattering models for the Mars Advanced Radar for Subsurface and Ionosphere Sounding (MARSIS). *Planet. Space. Sci.* **52**, 149-156 https://doi.org/10.1016/j.pss.2003.08.020.

Plaut, J.J., Picardi, G., Cicchetti, A., Clifford, S., Edenhofer, P., Farrell, W., Federico, C., Frigeri, A., Heggy, E., Herique, A., Ivanov, A., Jordan, R., Kofman, W., Leuschen, C., Marinangeli, L., Nielsen, E., Ori, G., Orosei, R., Pettinelli, E., Phillips, R., Plettemeier, D., Safaenili, A., Seu, R., Stofan, E., Vannaroni, G., Watters, T., Williams, I., 2006. MARSIS subsurface sounding observations of the South Polar Layered Deposits. Lunar Planet. Sci. Conf. XXXVII, 1211.

Plaut, J.J., Picardi, G., Safaenili, A., Ivanov, A.B., Milkovich, S.M., Cicchetti, A., Kofman, W., Mouginot, J., Farrell, W.M., Phillips, R.J., Clifford, S.M., Frigeri, A., Orosei, R., Federico, C., Williams, I.P., Gurnett, D.A., Nielsen, E., Hagfors, T., Heggy, E., Stofan, E.R., Plettemeier, D., Watters, T.R., Leuschen, C.J., Edenhofer, P., 2007. Subsurface radar sounding of the South Polar Layered Deposits of Mars. Science 316 (5281), 92-95 http://science.sciencemag.org/content/316/5821/92.

Plesa, A.-C., Padovan, S., Tosi, N., Breuer, D., Grott, M., Wieczorek, M.A., Spohn, T., Smrekar, S.E., Banerdt, W.B., 2018. The thermal state and interior structure of Mars. Geophys. Res. Lett. 45, 12198-12209 https://doi.org/10.1029/2018GL080728.

Primm, K.M., Gough, R.V., Chevrier, V.F., Tolbert, M.A., 2017. Freezing of perchlorate and chloride brines under Mars-relevant conditions. Geochim. Cosmochim. Acta 212, 211-220 https://doi.org/10.1016/j.gca.2017.06.012.

Porcello, L. J. and 7 colleagues 1974. The Apollo lunar sounder radar system. IEEE Proceedings 62, 769–783.

Putzig, N.E., Mellon, M.T., Kretke, K.A., Arvidson, R.E., 2005. Global thermal inertia and surface properties of Mars from the MSG mapping mission. Icarus 173 (2), 325-341 https://doi.org/10.1016/j.icarus.2004.08.017.

Putzig, N.E., Smith, I.B., Perry, M.R., Foss, F.J., Campbell, B.A., Phillips, R.J., Seu, R., 2018. Three-dimensional radar imaging of structures and craters in the Martian polar caps. Icarus 308, 138-147 https://doi.org/10.1016/j.icarus.2017.09.023.

Ramirez, R.M., Craddock, R.A., 2018. The geological and climatological case for a warmer and wetter early Mars. Nature Geoscience 11, 230-237 https://doi.org/10.1038/s41561-018-0093-9.

Sasaki, Y., Shang, F., Kidera, S., Kirioto, T., Saho, K., Sato, T., 2017. Three-dimensional imaging method incorporating range points migration and Doppler velocity estimation for UWB millimeter-wave radar. IEEE Geosci. Remote Sens. Lett. 14 (1), 122-126, doi: 10.1109/LGRS.2016.2628909 https://doi.org/10.1109/LGRS.2016.2628909.

Schroeder, D.M., Steinbrügge, G., 2021. Alternatives to liquid water beneath the south polar ice cap of Mars. Geophys. Res. Lett. 48(19), e2021GL095912 https://doi.org/10.1029/2021GL095912.

Sihvola, A., 2000. Mixing rules with complex dielectric coefficients. Subsurface Sensing Technologies and Applications 1, 393-415 https://doi.org/10.1023/A:1026511515005.

Simpson, R.A., Fair, B.C., Howard, H.T., 1980. Microwave properties of solid CO_2. J. Geophys. Res. 85 (B10), 5481-5484 https://doi.org/10.1029/JB085iB10p05481.

Smirnov, N. V. 1939. Estimate of deviation between empirical distribution functions in two independent samples. (Russian). Bull. Moscow Univ. 2, 3–16.

Smith, I.B., Hayne, P.O., Byrne, S., Becerra, P., Kahre, M., Calvin, W., Hvidberg, C., Milkovich, S., Buhler, P., Landis, M., Horgan, B., Kleinböhl, A., Perry, M.R., Obbard, R., Stern, J., Piqueaux, S., Thomas, N., Zacny, K., Carter, L., Edgar, L., Emmett, J., Navarro, T., Hanley, J., Koutnik, M., Putzig, N., Henderson, B.L., Holt, J.W., Ehlmann, B., Parra, S., Lalich, D., Hansen, C., Hecht, M., Banfield, D., Herkenhoff, K., Paige, D.A., Skidmore, M., Staehle, R.L., Siegler, M., 2020. The Holy Grail: A road map for unlocking the climate record stored within Mars' polar layered deposits. Planet. Space Sci. 184, 104841 https://doi.org/10.1016/j.pss.2020.104841.

Smith, I.B., Lalich, D.E., Rezza, C., Horgan, B.H.N., Whitten, J.L., Nerozzi, S., Holt, J.W., 2021. A solid interpretation of bright radar reflectors under the Mars south polar ice. Geophys. Res. Lett. 48(15), e2021GL093618 https://doi.org/10.1029/2021GL093618.

Sori, M.M., Bramson, A.M., 2019. Water on Mars, with a grain of salt: Local heat anomalies are required for basal melting of ice at the south pole today. *Geophys. Res. Lett.* **46**, 1222-1231 https://doi.org/10.1029/2018GL080985.

Tanaka, K.L., Kolb, E.J., 2001. Geological history of the polar regions of Mars based on Mars Global Surveyor data: I. Noachian and Hesperian periods. Icarus 154, 3-21 https://doi.org/10.1006/icar.2001.6675.

Tanaka, K.L., Skinner, J.A., Dohm, J.M., Irwin, R.P., Kolb, E.J., Fortezzo, C.M., Platz, T., Michael, G.G., Hare, T.M., 2014. Geologic map of Mars. USGS Sci. Invest. Map 3292, scale 1:20,000,000.

Thomas, P.C., Calvin, W.M., Gierasch, P., Haberle, R., James, P.B., Sholes, S., 2013. Time scales of erosion and deposition recorded in the residual south polar cap of Mars. Icarus 225 (2), 923-932 https://doi.org/10.1016/j.icarus.2012.08.038.

Toner, J.D., Catling, D.C., Light, B., 2014. The formation of supercooled brines, viscous liquids, and low-temperature perchlorate glasses in aqueous solutions relevant to Mars. *Icarus* **233**, 36-47 https://doi.org/10.1016/j.icarus.2014.01.018.

Ulaby, F.T., Moore, R.K., Fung, A.K., 1981. Microwave Remote Sensing – Active and Passive, vol. II. Artech House, Norwood, 921-949.

Whitten, J.L., Campbell, B.A., 2018. Lateral continuity of layering in the Mars South Polar Layered Deposits from SHARAD sounding data. J. Geophys. Res. Planets 123, 1541-1554 https://doi.org/10.1029/2018JE005578.

Whitten, J.L., Campbell, B.A., Morgan, G.A., 2017. A subsurface depocenter in the South Polar Layered Deposits of Mars. Geophys. Res. Lett. 44, 8188-8195 https://doi.org/10.1002/2017GL074069.

Wray, J.J., Murchie, S.L., Bishop, J.L., Ehlmann, B.L., Milliken, R.E., Wilhelm, M.B., Seelos, K.D., Chojnacki, M., 2016. Orbital evidence for more widespread carbonate-bearing rocks on Mars. J. Geophys. Res. Planets 121, 652-677 https://doi.org/10.1002/2015JE004972.

Zuber, M.T., Phillips, R.J., Andrews-Hanna, J.C., Asmar, S.W., Konopliv, A.S., Lemoine, F.G., Plaut, J.J., Smith, D.E., Smrekar, S.E., 2007. Density of Mars' South Polar Layered Deposits. *Science* **317** (5845), 1718-1719 http://science.sciencemag.org/content/317/5845/1718.